THERMAL DISSOCIATION OF METHANE USING A SOLAR COUPLED AEROSOL FLOW REACTOR

Alan W. Weimer, Jaimee Dahl, and Karen Buechler
University of Colorado, Department of Chemical Engineering
Boulder, CO 80309-0424

Allan Lewandowski, Roland Pitts, and Carl Bingham
National Renewable Energy Laboratory
Golden, CO 80401-3393

Gregory C. Glatzmaier
Peak Design
Evergreen, CO 80439

Abstract

A solar-thermal aerosol flow reactor has been constructed, installed and tested at the High-Flux Solar Furnace (HFSF) at the National Renewable Energy Laboratory (NREL). "Proof-of-concept" experiments were successfully carried out for the dissociation and the dry reforming (with CO_2) of methane to produce hydrogen and carbon black, and syngas, respectively. Approximately 90% dissociation of methane was achieved in a 25-mm diameter quartz reaction tube illuminated with a solar flux of 2400 kW/m^2 (or suns). An improved reactor has been designed and is being constructed to obtain more complete kinetic and process data for scale-up. Preliminary economics for a 5,000,000 kg/yr solar-thermal hydrogen plant were evaluated using a discount cash flow analysis that required a 15% internal rate of return (IRR). If either product is the sole source of revenue, the required selling price for hydrogen was $23/MBtu and for carbon black it was $0.48/lb. If both products are sold, and carbon black is sold for $0.20/lb (typical tire applications), the required selling price for hydrogen was $13/MBtu. If carbon black is sold at the current market price for typical chemical/battery applications ($0.35/lb), the price for hydrogen is a very attractive $6/MBtu. Both the experimental and economic results are very encouraging and support further work to address the technical issues and to develop the process.

Introduction

The primary driver for the development of renewable energy strategies is current concern over the potential, irreversible environmental damage that may occur with the continued or accelerated use of fossil fuels. Movement toward a hydrogen (H_2) based economy is an essential component of an international program to address that concern and will, in addition, address concerns over pollution in cities and associated health costs. However, current methods for producing H_2 incur a large environmental liability because fossil fuels are burned to supply the energy to reform methane (CH_4). We propose an alternate strategy using highly-concentrated sunlight as the energy source that does not result in an increase of environmental liability. Indeed, it represents a route for utilizing current natural gas reserves that fixes carbon as well as increasing the energy content of the fuel. The research presented here is oriented at developing a cost-effective, solar-thermal method of deriving H_2 from natural gas.

Objectives

The long-term objectives of the project are (1) to develop a technical and economic understanding of the benign synthesis of hydrogen using solar-thermal driven aerosol processing of natural gas; and (2) if technically and economically feasible, to develop the process with industrial partners.

Shorter-term objectives include (1) preliminary "proof-of-concept" experiments; (2) the design, fabrication, installation, and evaluation of an improved reactor system with in-line analytical characterization of the produced hydrogen-rich gas and measured flows allowing material balance closure – the design incorporating a secondary solar concentrator to increase solar efficiency and to increase attainable system temperatures; (3) an improved understanding of the process through preliminary math model development/experimental validation and economic/environmental impact analysis; (4) analytical characterization to assess the value of the produced carbon black under varying processing conditions (solar intensities, flow rates, etc.); and (5) dissemination of information via oral presentations at technical meetings and publications in peer-reviewed research journals.

Background

Steinberg [1986, 1987, 1994, 1995, 1998, 1999] and Steinberg and co-workers [Steinberg and Cheng, 1989] have been major proponents of the thermal decomposition of CH_4 process for H_2 production. Methane (CH_4) is dissociated to carbon (C) black and H_2 according to:

$$CH_4 \rightarrow C + 2H_2 \qquad \Delta H_{298K} = 74.9 \text{ kJ/mol} \qquad (1)$$

Methane (CH_4) is a preferred choice for the production of H_2 from a hydrocarbon because of its high H to C ratio (H/C = 4), availability, and low cost. Furthermore, the C produced can be sold as a co-product into the carbon black market (inks, paints, tires, batteries, etc.) or sequestered,

stored, and used as a clean fuel for electrical power generation. The sequestering or storing of solid C requires much less development than sequestering gaseous CO_2.

Gibbs free energy minimization calculations have been carried out (P = 0.1 MPa; 873 K ≤ T ≤ 2273 K) for the CH_4 dissociation system (i.e. CH_4 + heat ➔ equilibrium products) to determine equilibrium products. The concentrations of chemical species reaching a state of chemical equilibrium from reaction or partial reaction at atmospheric pressure for various reaction temperatures have been calculated using the F*A*C*T equilibrium code EQUILIB [Thompson et al., 1985]. Thermodynamically favored products (Figure 1) indicate dissociation above 600 K and that temperatures T > 1600 K are required to achieve nearly complete dissociation. Although not shown, trace products at 1600 K include C_2H_2, C_2H_4, C_4H_8, C_3H_6, C_2H_6, and other species at concentrations < 40 ppm.

There are several alternatives to supply the energy required to drive reaction (1). In the commercial "Thermal Black Process" [Donnet, 1976], the energy is provided by burning CH_4 with air to heat a fire brick furnace to temperatures as high as 1673K. Once hot, the air is shut off

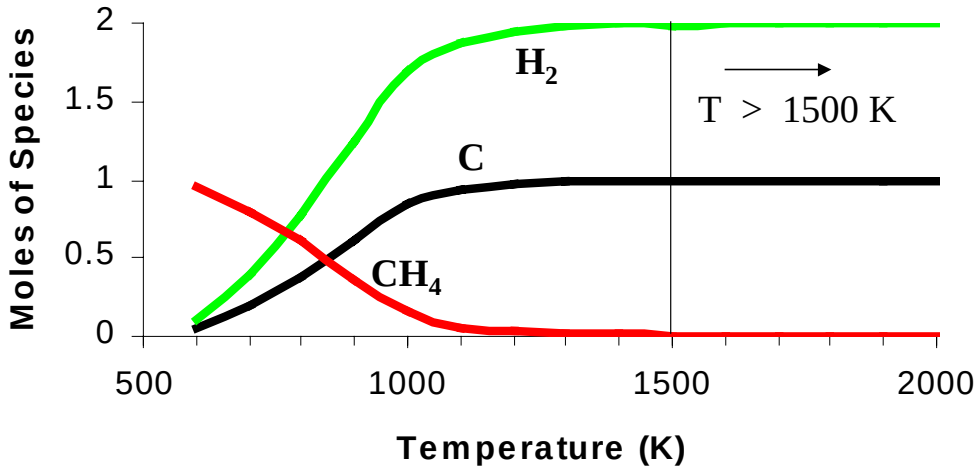

Figure 1. Primary Methane Decomposition Equilibrium Products P = 0.1 MPa

and the CH_4 decomposes according to reaction (1) until the wall temperature drops to below 1073 K. The system is operated semi-continuously with CH_4 burned in one sequence of the cycle to supply the heat necessary to carry out the decomposition in the second sequence. This process has been practiced for many years for the production of carbon black. The H_2 produced is used as a fuel to heat the furnace and the CH_4 feedstock.

Pohleny and Scott (1962) used a fluidized bed/riser thermal decomposition reactor process that uses iron oxide for heat transfer and as a catalyst. Carbon collected on the iron oxide particles in the fluidized bed is burned off in the riser reactor for reheating the iron oxide particles that are

recirculated to the endothermic fluidized bed reactor. Hydrogen is produced continuously by the decomposition occurring in the fluidized bed.

Gaudernack and Lynum (1996) and Bromberg et al. (1998) used a plasma torch to supply the necessary energy to decompose CH_4 and produce a continuous stream of H_2. The plasma gas is H_2 that is recirculated from the process. Although no CO_2 is liberated from the process reactor itself, electricity is required to produce the plasma. When the electrical power is produced from natural gas fuel combustion, even in an efficient combined cycle plant, the overall thermal efficiency is significantly reduced and the CO_2 emission per unit energy is significantly increased.

In another process [Steinberg, 1995a], a molten metal bath reactor (such as tin or copper) is used to transfer heat to CH_4 that is bubbled through the molten metal. The reactor is heated by combustion products (CH_4 or H_2 burned with air) that flow through an internal heat exchanger. In this process, it is proposed to capture carbon in the liquid metal and to separate it from the metal by density difference, skimming the carbon off from the surface much as slag is skimmed off the surface of molten iron in a conventional blast furnace.

Although thermodynamics can predict when a reaction will not occur, it cannot predict whether a reaction will indeed occur in practice. Activation energies, transport processes (e.g. heating rate), and other reaction kinetic considerations are needed in order to determine if a reaction can be completed for a given amount of time in a chemical reactor design. Such kinetic data have been reported for reaction (1) using electrically-heated pilot-scale aerosol flow reactors [Matovich, 1977].

Matovich (1977) showed that the decomposition of CH_4 could be carried to completion in a short residence time aerosol reaction tube at temperatures $T > 2088$ K. The reactor consisted of a 0.0762-m diameter x 0.914-m long (3 inch ID x 3 ft long) graphite aerosol reaction tube heated indirectly by radiation from external electrodes heated directly by electrical resistance. Later studies included work carried out in 0.305-m ID x 3.66-m long (1 ft ID x 12 ft long) reaction tubes [Lee et al., 1984]. A small amount of carbon black was introduced in the CH_4 feed stream to serve as a radiation-absorbing target to initiate the pyrolytic reaction. Due to the high temperatures involved and the difficulty in heating a gas to those temperatures (by convection from the reactor walls), the carbon particles are the key to this process.

Reactions were carried out in the temperature range of $1533 < T < 2144$ K with residence times between approximately 0.1 and 1.5 seconds. The fraction of CH_4 dissociated was determined by measuring the thermal conductivity of the effluent gas after filtering the carbon black particles from the sample. Hydrogen (H_2) flowed radially through a porous reaction tube, providing a fluid-wall to prevent carbon black from depositing on the wall. The residence time in the reactor was controlled by the inlet flow of CH_4, the radial flow of H_2, and the reactor temperature. Some reported results [Matovich, 1977] where data were available for both a minimum residence time ($t_{r(min)}$) of 0.2 s and a maximum residence time ($t_{r(max)}$) of 1 s are summarized in Figure 2. It is clear from these results that residence time has little effect on dissociation for temperatures $T > 1900$ K and that complete dissociation can be achieved in aerosol flow reactors for temperatures greater than approximately 2100 K for reaction times of $t = 0.2$ s.

The process investigated here is the high-temperature thermal dissociation of CH_4 using a solar-thermal aerosol flow reactor. The energy required to drive reaction (1) is supplied by concentrated sunlight. An experimental reactor apparatus was constructed and interfaced to NREL's HFSF [Jenkins et al., 1996; Lewandowski, 1993; Lewandowski et al., 1991; and Pitts et al., 1993]. There is no need for auxiliary cooling at the optical source. The reactor is operated as a cold wall process, because the beam is delivered directly on target. In addition, the control of solar radiation (on/off) is almost instantaneous. Absorbing surfaces exposed to concentrated solar radiation can reach temperatures of between 1000 K and 3000 K in fractions of a second. The process produces H_2 using high-efficiency direct solar-thermal heating with no associated CO_2 generation.

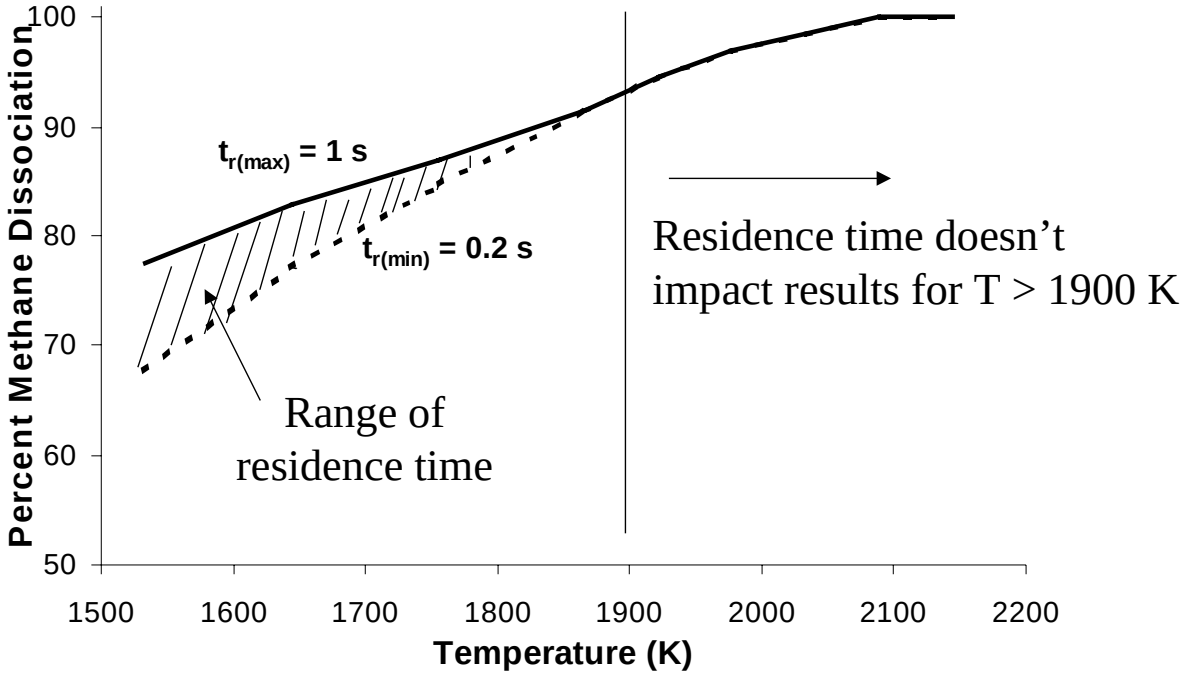

Figure 2. Effect of Residence Time & Temperature

Theoretical Work

In order to gain a better understanding of the reaction kinetics in the solar-thermal reactor, a model was developed to describe the reactor developed by Matovich (1977). The data obtained by Matovich (1977) are the only know data for complete dissociation of methane to carbon and hydrogen at high temperatures. The model incorporates a kinetic model to describe the rate of conversion as well as a gas phase energy balance and a carbon particle energy balance. The following assumptions are made: (1) both the carbon particle and the gas temperature vary only

in the axial direction; (2) all gases are transparent to radiation [Kreith and Black, 1980]; (3) radiative emissivities and absorptivities are equal for the carbon particles [Kreith and Black, 1980]; (4) the carbon particles and the gas stream are moving at the same velocity; (5) the reactor operates at steady state; and (6) the feed gas is pure methane. The nomenclature for the next sections is located at the end of this document.

Kinetic Model

A typical rate expression for decomposition was used to model kinetics [Weimer, 1997]:

$$\frac{dX}{dt} = k(1-X)^a \tag{2}$$

Using the chain rule,

$$\frac{dX}{dz} = \frac{k(1-X)^a}{v_g} \tag{3}$$

where the reaction rate, k, is defined by the Arrhenius expression:

$$k = k_o \exp\left(\frac{-E_a}{RT_g}\right) \tag{4}$$

Due to the nonlinearity of the Arrhenius expression, an interaction between k_o and E_a arises. This interaction is reduced by a transformation of T_g in the expression [Himmelblau, 1970]:

$$k = k_o^* \exp\left[\frac{-E_a^*}{R}\left(\frac{1}{T_g} - \frac{1}{T_o}\right)\right] \tag{5}$$

where T_o = 1200K. T_o is an arbitrarily chosen temperature that is within the range of temperatures occurring in the reactor. The resulting kinetic expression is

$$\frac{dX}{dz} = \frac{k_o^* \exp\left[\frac{-E_a^*}{R}\left(\frac{1}{T_g} - \frac{1}{T_o}\right)\right](1-X)^a}{v_g} \tag{6}$$

Carbon Particle and Gas Phase Thermal Energy Balances

An energy balance around an arbitrary volume element of the gas phase was made. The gas phase is heated by the reactor wall, the hydrogen gas introduced through the porous reactor wall,

and the carbon particles. The sources of the energy generated and consumed are shown in Figure 3.

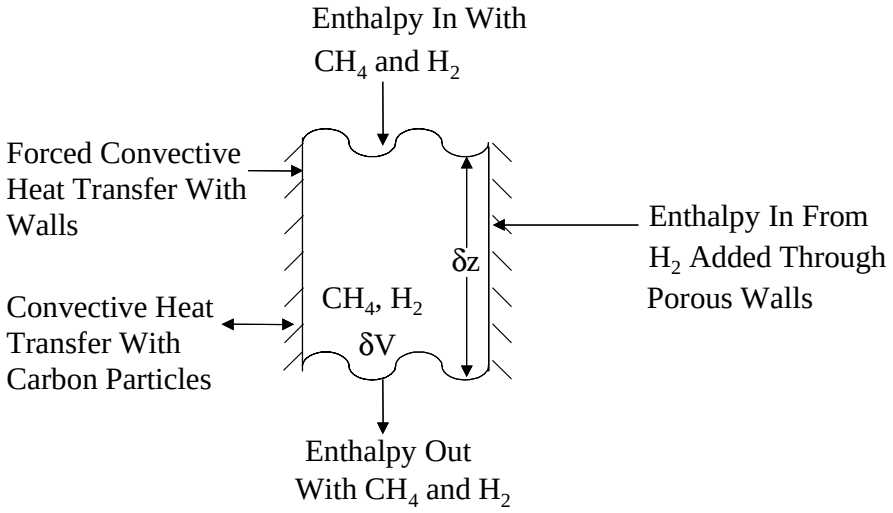

Figure 3. Schematic of Heat Transfer in Gas Phase

By combining these sources of energy one can develop an expression that describes the change in gas temperature along the distance down the reactor:

$$\frac{dT_g}{dz} = \frac{F^o_{CH4}[H_{CH4}(@T_g) - 2H_{H2}(@T_g)]\frac{dX}{dz} + g\int_{T_g}^{T_w} C_{pH2}dT + h_w\pi d_i(T_w - T_g) + h_p\frac{a_c F_c M_{wc}}{v_g V_c \rho_c}(T_c - T_g)}{F_{CH4}C_{pCH4} + F_{H2}C_{pH2}} \qquad (7)$$

The first term in the numerator of the right hand side accounts for the hydrogen formed by reaction, the second term describes the energy brought in with the hydrogen added through the walls, the third term accounts for the convective heat transfer between the walls and the gas stream, and the last term describes the convective heat transfer between the particles and the gas phase.

A similar balance was conducted for a cloud of carbon particles. The particles absorb heat from the walls and transfer that energy to the gas stream. The components of the energy balance are shown in a schematic diagram in Fig. 4.

A description of the change in carbon particle temperature over the distance of the reactor is given by:

$$\frac{dT_c}{dz} = \frac{-F^o_{CH4}H_c(@T_c)}{F_c C_{pc}}\frac{dX}{dz} + \frac{-h_p a_c A_i n_c(T_c - T_g) + \varepsilon_c \sigma a_c A_i n_c(T_w^4 - T_c^4)}{F_c C_{pc}} \qquad (8)$$

The first term on the right hand side of equation (8) describes heat generated by the carbon formed by reaction. The second term on the right hand side accounts for the convective heat

transfer between the particles and the gas, and also the radiative heat transfer between the reactor walls and the particles.

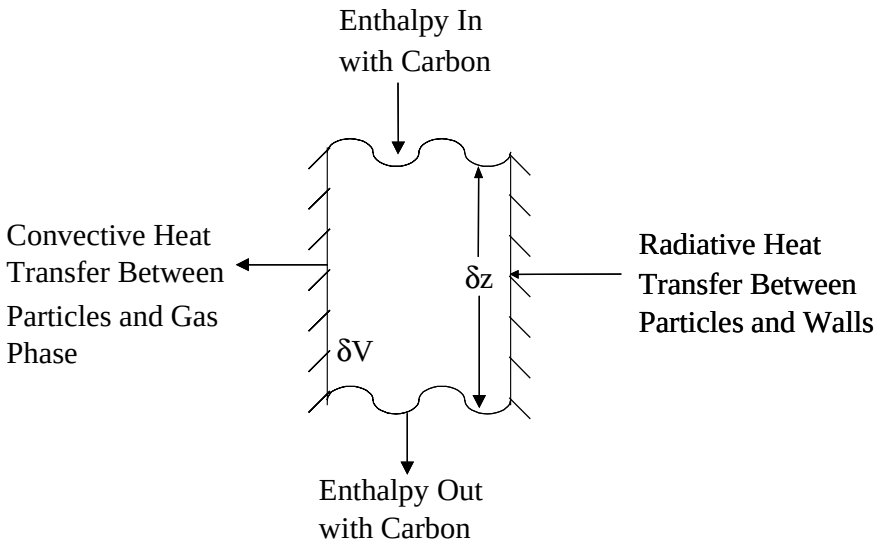

Figure 4. Schematic of Heat Transfer in a Cloud of Carbon Particles

Supporting Equations

Several equations were used to define the variables in the ordinary differential equations. The heat transfer coefficient between the gas phase and the carbon particles is defined as:

$$h_p = \frac{k_g}{R_o} \tag{9}$$

where k_g is the thermal conductivity of the gas and R_o is the radius of a carbon particle.

For surface temperatures from 1173 K to 2473 K, the convective coefficient between the gas phase and the reactor walls is [Roberts et al., 1971]:

$$h_w = 0.034\left[\frac{k_g(@T_f)}{d_i}\right]\left[\frac{F_g M_{wg} d_i}{A_i \mu_g(@T_f)}\right]^{0.8}\left(\frac{T_g}{T_f}\right)^{0.8}\left[\frac{C_{pg}(@T_f)\mu_g(@T_f)}{k_g(@T_f)M_{wg}}\right]^{0.4}\left(\frac{L}{d_i}\right)^{0.1} \tag{10}$$

where T_f is the film temperature (arithmetic average of the gas temperature and wall temperature), F_g is the molar flow rate of the gas, M_{wg} is the molecular weight of the gas, μ_g is the viscosity of the gas, and C_{pg} is the heat capacity of the gas.

The molar flow rates for each species are as follows:

$$F_{CH_4} = F^o_{CH_4}(1 - X) \tag{11a}$$

$$F_c = XF^o_{CH_4} + 0.1 \text{mol/s} \tag{11b}$$

$$F_{H_2} = 2XF^o_{CH_4} + fz \tag{11c}$$

The second term on the right hand side of Equation (11b) is an estimate of the amount of carbon added to the system initially to initiate the reaction. The second right-hand-side term of Equation (11c) accounts for the hydrogen added through the porous walls. It was assumed that the quantity of hydrogen entering the reactor was evenly distributed over the length of the reactor tube.

The molecular weight of the gas phase can be calculated as follows:

$$M_{wg} = \frac{\sum_{gas(i)} F_i M_{wi}}{\sum_{gas(i)} F_i} \tag{12}$$

Similarly, the specific heat capacity of the gas phase can be calculated as:

$$C_{pg} = \frac{\sum_{gas(i)} F_i C_{pi}}{\sum_{gas(i)} F_i} \tag{13}$$

The thermal conductivity of the gas phase can be calculated by:

$$k_g = \frac{\sum_{gas(i)} F_i k_i M_{wi}^{1/3}}{\sum_{gas(i)} F_i M_{wi}^{1/3}} \tag{14}$$

The viscosity of the gas phase can be calculated as:

$$\mu_g = \frac{\sum_{gas(i)} F_i \mu_i M_{wi}^{1/3}}{\sum_{gas(i)} F_i M_{wi}^{1/3}} \tag{15}$$

The velocity of the gas phase can be calculated by:

$$v_g = \frac{\sum_{gas(i)} \frac{F_i}{\rho_i}}{A_i} \tag{16}$$

Data found in Yaws (1999), Touloukian (1970, 1975), and FACT (1999) are used to calculate the viscosities, heat capacities, and thermal conductivities of hydrogen and methane.

Simulations

The parameters used for simulating the reactor are listed in Table 1. These parameters, as well as the experimental conditions, such as furnace wall temperature (T_w), feed gas flow rate (F^o_{CH4}), and flow rate of H_2 added through the reactor walls (f), are used with equations 6, 7, and 8 and the supporting equations to form a system of coupled ordinary differential equations and algebraic equations that are solved simultaneously. A best-fit model is obtained by varying the kinetic constants (a, k_o^*, and E_a^*). The Gauss-Newton method [Chapra and Canale, 1988] is used, which minimizes the sum of the squares of the residuals between the conversions reported by Matovich (1977) and the conversions calculated by equation (6). A constraint was placed in the model requiring approximately 100% conversion for wall temperatures at or above 2089K for methane feed flow rate of 0.0189 mol/s. In addition to conversion profiles, the simulation outputs gas phase and carbon particle temperature profiles.

Results and Discussion

Intrinsic Kinetics

All data with a conversion of 90% or less were fit. This resulted in fitting 22 data points in the wall temperature range of 1533-1977 K as well as forcing the model to predict approximately 100% conversion at the point corresponding to a wall temperature of 2089 K and an initial methane flow rate of 0.0189 mol/s. A comparison between the conversions determined experimentally by Matovich and the conversions calculated theoretically using the model is shown in Figure 5.

These conversions were calculated using the following best-fit kinetic parameters: a=4.4, $k_o=6x10^{11}$ s^{-1}, and $E_a=208 \pm 65$ kJ/mol. These three parameters had the best fit to the experimental data, but there were several other points with comparable fits. The activation energy predicted by this model is lower than that reported in the literature. The fine carbon particles that are fed into the reactor and are formed by reaction have a significant amount of surface area. They catalyze the reaction and thus decrease the activation energy [Steinberg, 1998].

Using these parameters, the model was run for various reactor wall temperatures and initial methane molar flow rates. A plot of feed methane molar flow rate versus final conversion for several wall temperatures is shown in Figure 6.

Due to the large number of data points, profiles from only a selection of points will be presented. The conversion profiles for an initial methane molar flow rate of 0.0566 mol/s are shown in Figure 7. The wall temperature was varied between 1533 and 1922 K. Conversion profiles for a wall temperature of 1644 K, with the initial methane molar flow rate varying from 0.0189 to 0.0944 mol/s, are portrayed in Figure 8.

Table 1. Parameters Used in Reactor Simulation

Parameter	Value	
a	4.4	
a_c	3.14×10^{-8}	m^2
A_i	4.56×10^{-3}	m^2
d_i	0.076	m
E_a	208	kJ/mol
F	2.36×10^{-3}	m^3/s
F^o_{CH4}	0.0189 - 0.0944	mol/s
K_o	6×10^{11}	s^{-1}
L	0.914	m
M_{wc}	0.012	kg/mol
R	8.314	J/mol K
R_o	5×10^{-5}	m
T_w	1533 - 2144	K
V_c	5.24×10^{-13}	m^3
ε_c	1	
ρ_c	2270	Kg/m^3
σ	5.67×10^{-8}	$W/m^2 K^4$

Initial Conditions for Ordinary Differential Equations		
T_g	298	K
T_c	298	K
X	0	

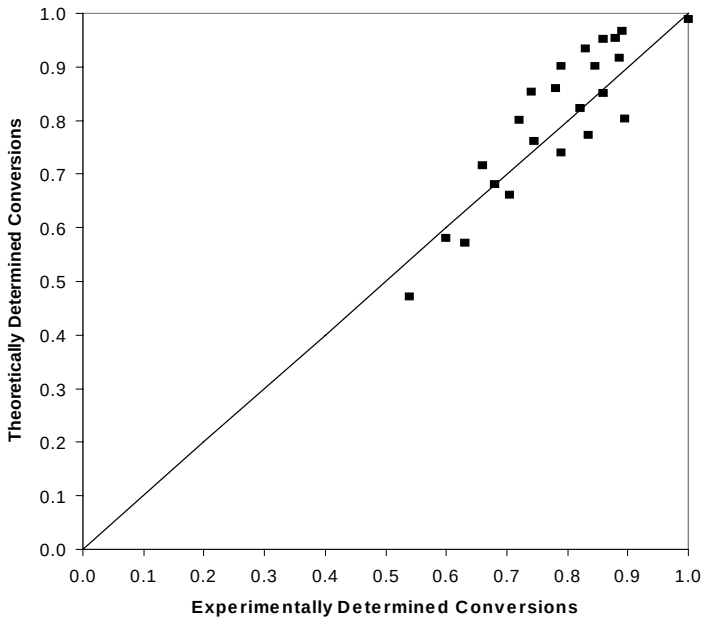

Figure 5. Comparison of Theoretically and Experimentally Determined Conversions

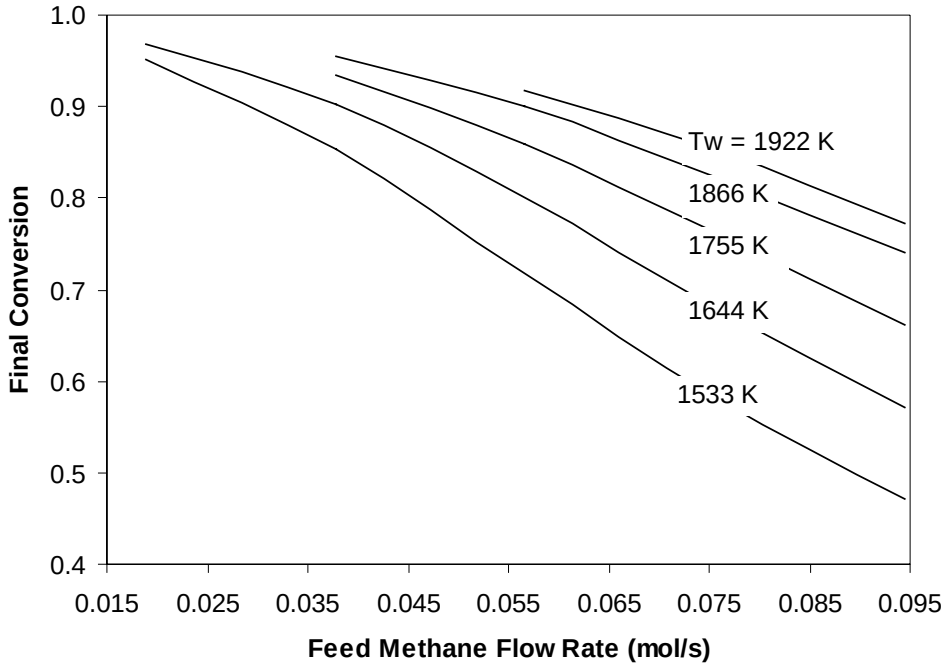

Figure 6. Feed Methane Flow Rate Versus Final Conversion for Various Wall Temperatures

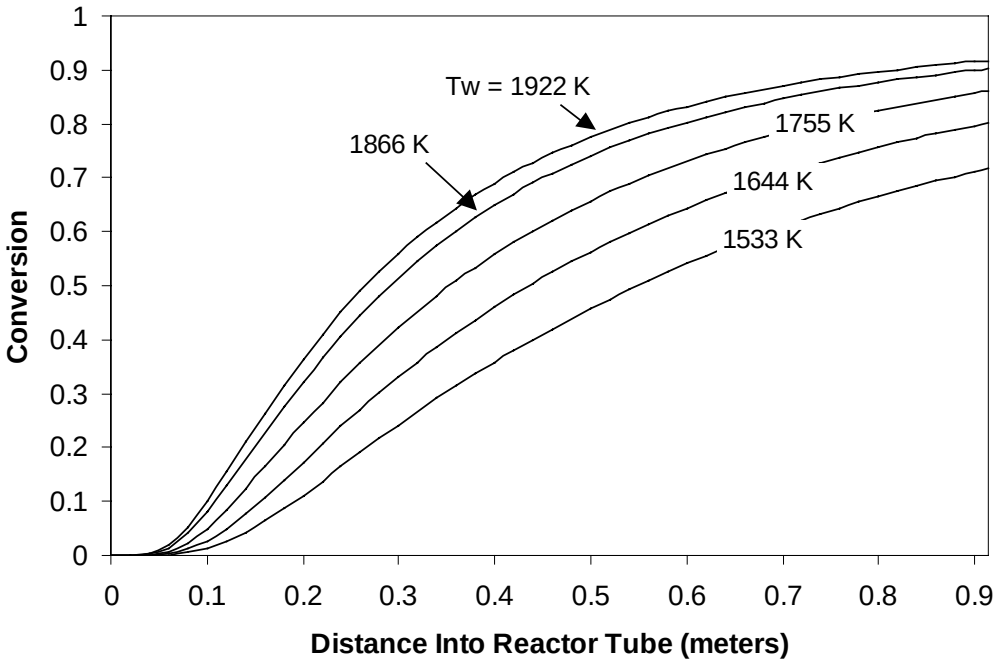

Figure 7. Conversion Profiles for F^0_{CH4} = 0.0566 mol/s

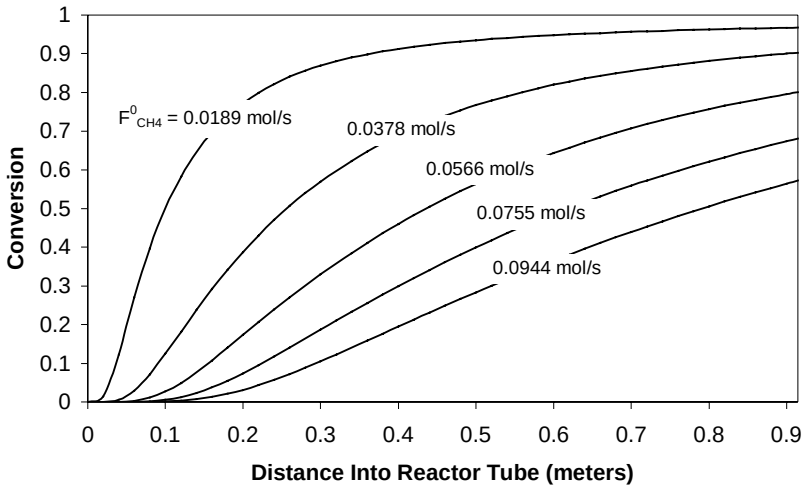

Figure 8. Conversion Profiles for T_w = 1644 K

Temperature Profiles

The best-fit kinetic constants (a=4.4, $k_o=6x10^{11}$ s^{-1}, and E_a=208 kJ/mol) were used to find temperature profiles for various reactor wall temperatures and initial methane molar flow rates. The gas temperature profiles and carbon particle temperature profiles for wall temperatures of 1533 and 2144 K and initial methane molar flow rate of 0.0566 mol/s are shown in Figure 9.

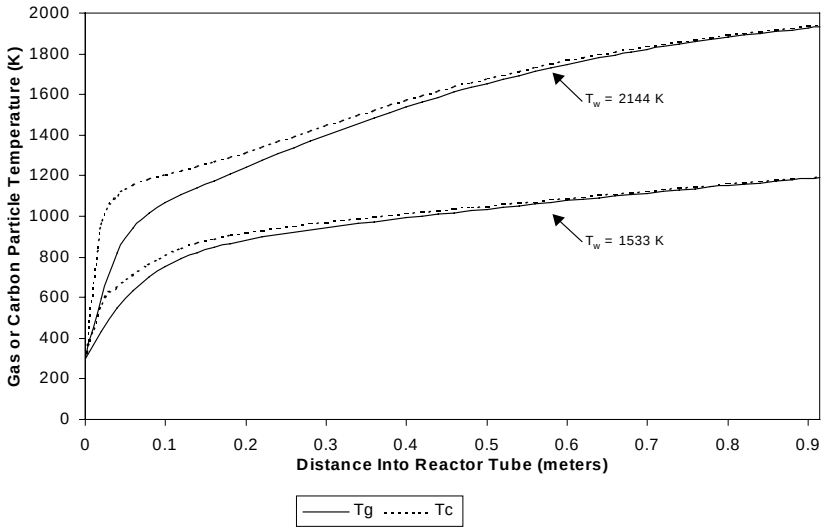

Figure 9. Gas and Carbon Particle Temperature Profiles for F^0_{CH4} = 0.0566 mol/s

It is evident from these profiles that the temperature of the gas stream very closely follows the temperature of the carbon particles. The heating rate for both the gas stream and the carbon particles is extremely fast for the first 0.1 m of the reactor tube. The heating rate then slows as the streams move through the remainder of the reactor until both streams reach approximately the same temperature at the end of the reactor. The final temperature of both the gas stream and the carbon particles is slightly lower than the wall temperature.

Experimental Work

High-Flux Solar Furnace

The HFSF facility (Figure 10) at NREL in Golden, CO was used for this research. NREL is the primary national laboratory in the United States for renewable energy research. The HFSF uses a series of mirrors that concentrate sunlight to a focused beam at maximum power levels of 10 kW into an approximate diameter of 10 cm. The solar furnace's long focal length and its off-axis design give researchers flexibility and control over the delivered flux. It operates with a heliostat that has an area of 31.8 m^2 and a 92% solar-weighted reflectivity. The heliostat reflects sunlight to a primary concentrator consisting of 25 hexagonal facets that are spherical mirrors ground to a 14.6-m radius of curvature. The total surface area of the primary concentrator is 12.5 m^2 and it reflects radiation from the entire solar spectrum (300 nm to 2500 nm). Under optimal conditions, the primary concentrator can achieve maximum flux intensities of 2,500 suns. Secondary concentrators that achieve intensities of more than 20,000 suns and refractive designs approaching 50,000 suns can be installed at the primary concentrator's focal point to increase the intensity further. The furnace is easily capable of delivering flux densities on the order of 100-1000 W/cm^2. No secondary solar concentration was used in these studies.

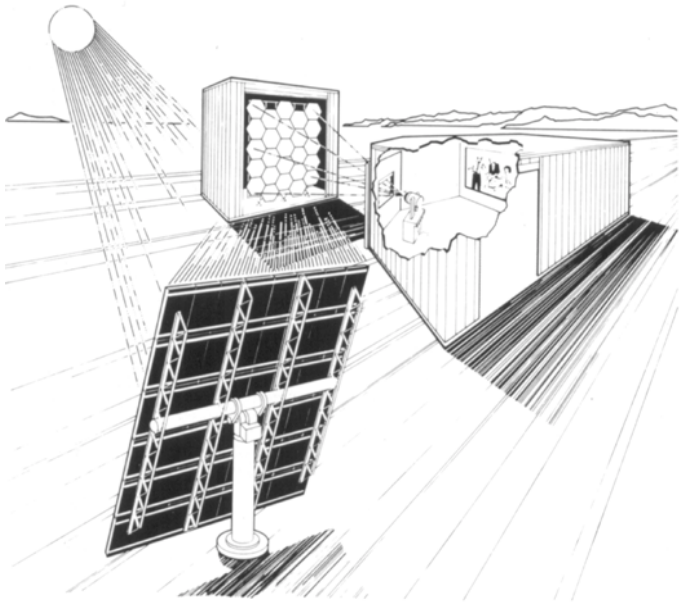

Figure 10. High-Flux Solar Furnace Schematic

Reactor System

Proof-of-concept experiments were carried out using a modified reactor system originally built for previous experiments in fullerene production [Mischler et al., 1997]. The reactor consists of a particle and gas feed mechanism, quartz reactor tube, an internal graphite "target" feed tube, and a filter housing. The reactor operates at atmospheric pressure with gas flow driven and controlled through a series of mass flow controllers. An in-line Horiba model TCA-300 H_2 detector was inserted downstream of the particle filter. This detector is based on thermal conductivity measurements and was calibrated for 5 % H_2 in argon (Ar). Gas samples were also taken and analyzed using an off-line gas chromatograph (GC). CH_4 and produced H_2 were kept outside flammability limits by operating with a dilute 5% CH_4 in Ar feed gas mixture and a pure Ar purge stream. The temperature inside the quartz tube reactor is exceedingly difficult to determine. However, the temperature of the quartz tube is carefully monitored using an infrared camera positioned on the side of the reactor. The quartz temperature is monitored to avoid warping or even melting the reactor wall with concentrated sunlight. A schematic of the reactor system is shown in Figure 11.

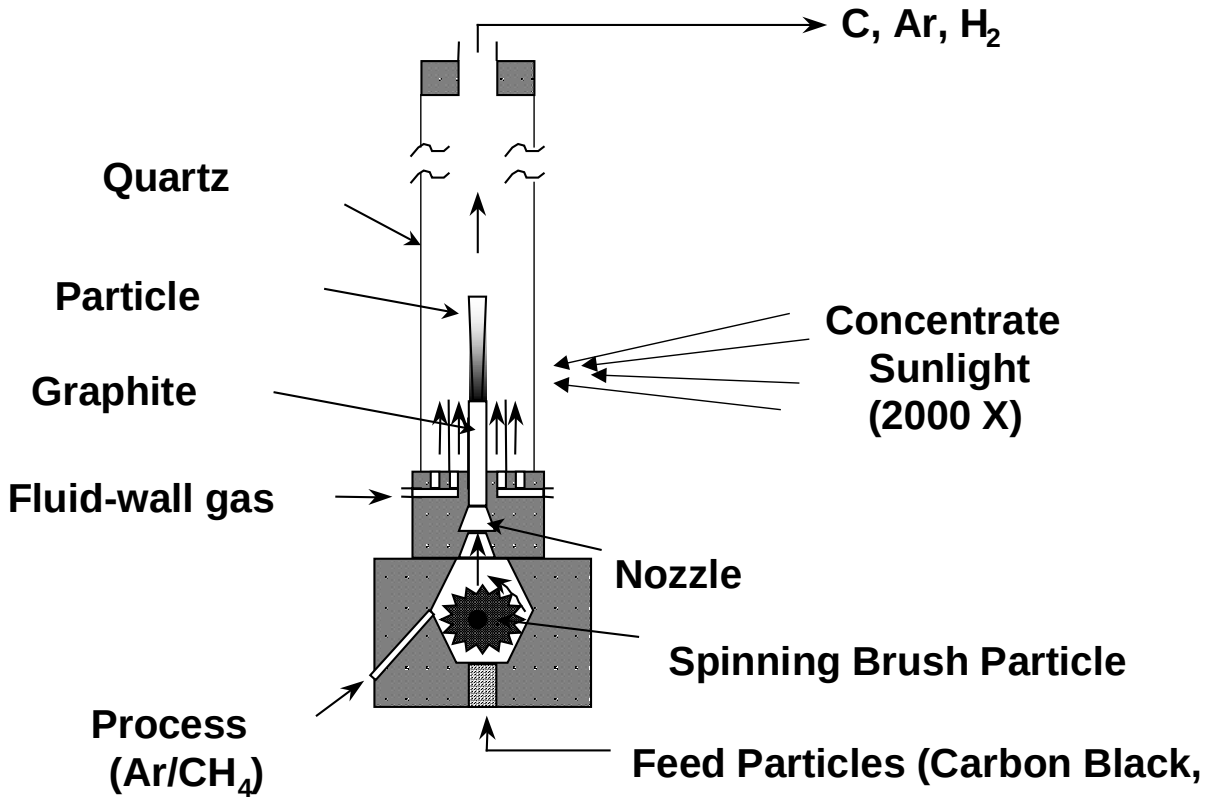

Figure 11. Schematic of Solar-Thermal Aerosol Flow Reactor

A key aspect of the reactor operation is the heating means for the feed CH_4. The reactor has been designed for three alternative heating methods: (1) heating a 6 mm OD x 3 mm thick "target" graphite tube with concentrated sunlight, the heated target then heating the CH_4-containing feed gas by conduction; (2) heating the "target" graphite tube, but with radiation absorbing fine carbon black particles suspended in the CH_4-containing feed gas stream so the inside wall of the "target" radiates to the flowing particles that subsequently heat the flowing feed gas by particle surface conduction in addition to the wall conduction; and (3) heating the suspended carbon black particles directly with concentrated sunlight, the sunlight directed above the top of thegraphite tube. Alternatives (2) and (3) involve volumetric absorption of light by a gas-solid suspension. The graphite tube can be seen contained within the quartz tube reactor assembly as shown in Figure 12. The quartz tube extends beyond the limits of the concentrated solar flux provided by the HFSF. The quartz tube was positioned at the nominal focus along the optical axis of the HFSF with its axis "vertical".

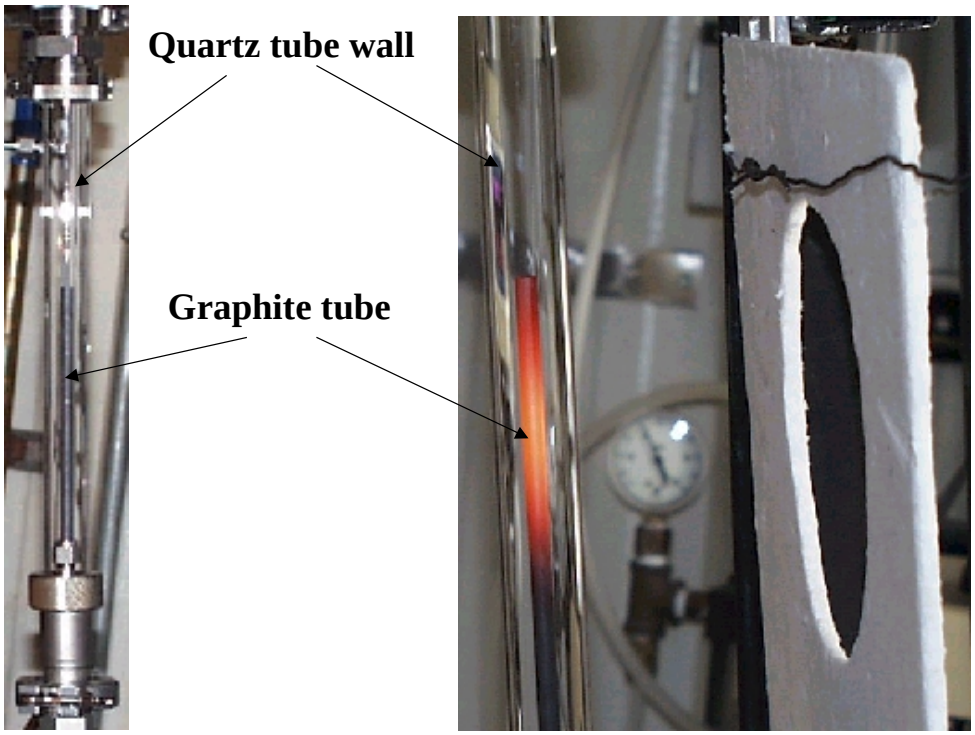

a. **b.**

Figure 12. Reactor Tube Assembly: a. before heating, b. immediately after heating (shutter closed)

The particle suspension is generated in a feed mechanism located below the quartz tube (see Figure 13). Lightly compacted carbon black particles ("Shawinigan^{TM}" acetylene carbon black; product of Chevron Chemical Co., Houston, TX) are fed against a rotating steel brush that conveys the particles to a space where they are mixed with the 5% CH_4/Ar feed gas. The suspension then flows through a set of nozzles that destroy any particle agglomerates. The nozzle size varies between 0.33 mm and 0.64 mm. Before the particle cloud passes through the focal

area, two streams of “sweep” Ar gas are “wrapped” around the gas-solid suspension. This “fluid-wall” is designed to prevent particles from reaching the quartz glass in locations where heating by the highly concentrated sunlight might soften or melt the tube. The gas and particles are fed from bottom to top of the quartz reactor. With the ratio of “sweep” Ar to feed 5% CH_4/Ar on the order of 10:1, the overall percentage of CH_4 or H_2 was relatively low for these proof-of-concept experiments. These low concentrations are used as a safety precaution for initial studies. A side view of the reactor assembly above the particle feeding system is shown in Figure 14.

Figure 13. Particle Feeding System (below reactor assembly)

During one set of experiments, the reactant gas was fed at a rate of 0.2 standard liters per minute (SLM) into the graphite reaction tube while the annular argon “purge” gas flowed at a rate of 2 SLM. The adjusted molar concentration of inlet CH_4 accounting for a combined reactant “purge” gas stream near the exit of the graphite reaction tube was 0.45%. The estimated flux of concentrated sunlight heating the graphite reaction tube target was 1200 kW/m^2. A temperature of 1550 K was measured inside the graphite tube using a Type C thermocouple positioned in the center of the hot zone. The length of the hot zone was 50 mm long. The residence time of the methane in the hot zone of the reactor tube was 0.019 seconds. Any fed and synthesized carbon black were separated downstream of the reactor using a HEPA filter. A calibrated thermal conductivity detector located downstream of the filter indicated a hydrogen concentration of 0.27 mole% H_2 in argon. This corresponded to a methane conversion to carbon and hydrogen of 30% according to reaction (1).

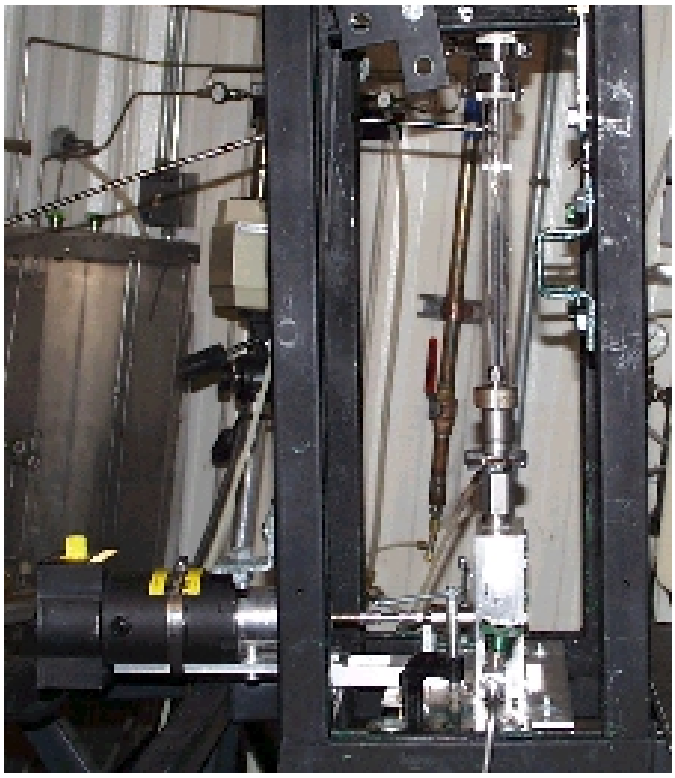

Figure 14. Reactor Assembly (above particle feeding system)

Proof-of-concept Results and Discussion

The process parameters described above were repeated with the exception that no carbon particles were fed in the process. The product gas was measured by the calibrated thermal conductivity detector to have a hydrogen content of 0.16% H_2, corresponding to a reduced methane conversion of 18%. Carbon black produced according to reaction (1) was collected in a downstream filter and analyzed by transmission electron microscopy (TEM). The carbon black was amorphous and was comprised of carbon particles having a size in the range of 20 to 40 nanometers. These results indicated that the feeding of fine carbon black particles to the process increases the conversion of the thermal dissociation of methane for low temperatures. These results also indicate that amorphous fine carbon black powder is produced in the process and the process provides an in-situ method of generating carbon black radiation absorbers in the reactor (without having to feed it).

The next set of experiments was performed to determine the effect of varying the solar flux. The reactant gas flowed at a rate of 0.2 SLM and had a composition of 10 mole% CH_4 in argon. The annular "purge" argon flow rate was 1 SLM and no carbon particles were fed. The adjusted molar concentration of CH_4 accounting for a combined reactant "purge" gas stream near the exit of the graphite reaction tube was 1.67%. The estimated flux of concentrated sunlight heating the graphite reaction tube target was varied as 1170 kW/m^2, 1780 kW/m^2, 2060 kW/m^2, and

2350 kW/m^2. The corresponding temperatures in the reaction tube were 1550, 1730, 1820, and 1900 K, respectively. The residence time varied in the range of 0.019 to 0.015 seconds, respectively. The response of the hydrogen content in the flowing product gas stream resulting from the solar flux changes is shown in Figure 15. The conversion of methane according to reaction (1) was calculated from the measured concentration of H_2 and was 7%, 38%, 43%, and 47%, respectively. These results indicate that an increase in the solar flux results in an increase in the thermal dissociation (conversion) of methane to H_2 and carbon black.

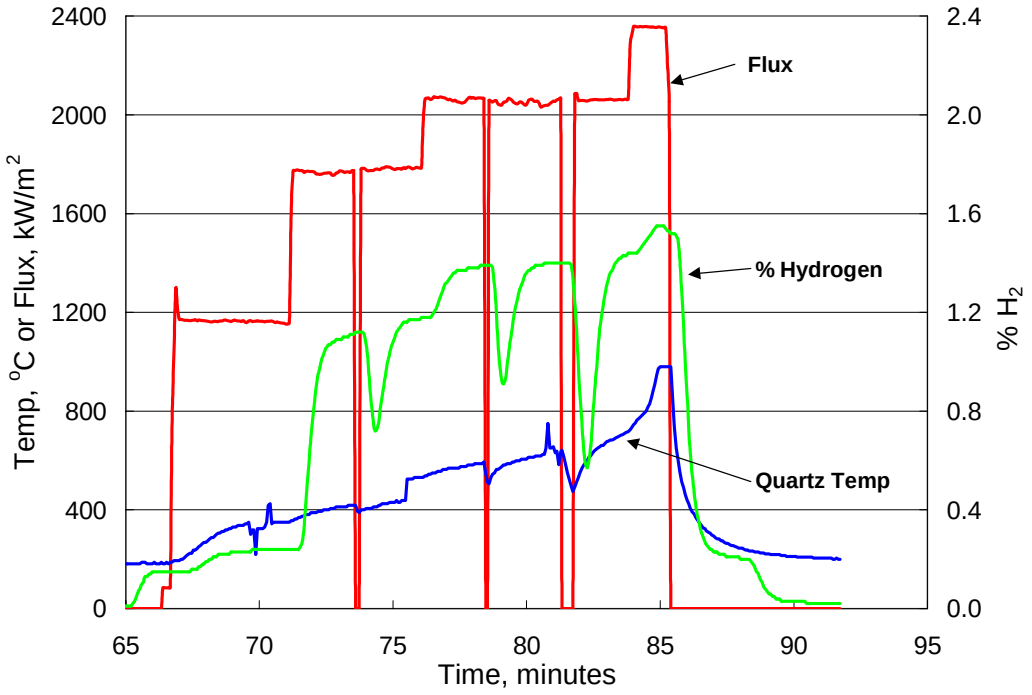

Figure 15. Signal Response to Solar Flux (1.7% CH_4 and no particle feed)

Once again, the reactant gas was fed at a rate of 0.2 standard liters per minute (SLM) into the graphite reaction tube while the annular argon "purge" gas flowed at a rate of 2 SLM. However, in this set of experiments, the solar flux was increased from 1200 kW/m^2 (described previously) to 2430 kW/m^2. The temperature in the hot zone was measured to be 1915 K compared to 1550 K (described previously). The resulting concentration of H_2 (0.55 mole%) indicated a methane dissociation of 61% according to reaction (1). This result indicates that the higher solar flux results in a higher degree of dissociation (conversion) of methane.

The same process conditions were repeated, except that no carbon particles were fed to the reactor. The concentration of H_2 indicated that the dissociation of CH_4 was 36%. This illustrates that a decrease in dissociation results when carbon particles are not co-fed in the process to improve heat transfer.

The process conditions were repeated except reactant gas flow was decreased to 0.1 SLM, resulting in an adjusted molar concentration of CH_4 accounting for a combined reactant "purge"

gas stream near the exit of the graphite reaction tube of 0.24 mole%. A calculated residence time of 0.03 seconds resulted in a measured outlet hydrogen concentration of 0.4 mole% H_2 for a degree of dissociation of 84%. This experiment shows that high conversions (extents of dissociation) can be achieved in hundredths of a second for high reactor temperatures (1915 K) obtained using concentrated solar-thermal heating.

This set of experiments was run to determine the effect of using larger graphite tube sizes. Particles were fed and the reactant gas was fed at a rate of 0.2 standard liters per minute (SLM) into the graphite reaction tube while the annular argon "purge" gas flowed at a rate of 3 SLM. A 10 mm outside diameter graphite tube was used. An adjusted molar concentration of CH_4 accounting for a combined reactant "purge" gas stream near the exit of the graphite reaction tube was 0.91 mole%. The solar flux was 1523 kw/m^2, 1700 kW/m^2, and 1900 kW/m^2. The measured temperatures in the graphite reaction tube were 1650 K, 1710 K, and 1770 K and the corresponding reaction residence times were 0.064, 0.061, and 0.059 seconds, respectively. The concentrations of hydrogen determined from the thermal conductivity detector were 0.54 mole%, 0.83 mole%, and 1.14 mole%, respectively. During the course of the experiments, gas samples were taken in the outlet line and analyzed using an off-line gas chromatograph (GC). The following chemical compositions were determined, respectively: 0.65 mole%, 0.85 mole%, and 1.25 mole%. The GC results corresponded to a methane dissociation of 35%, 48%, and 70% conversion. This set of experiments indicated that different sizes of graphite reaction tubes could be used and that the experimental results using the thermal conductivity analysis were validated with the off-line GC.

The processing conditions described in the previous paragraph were repeated with the exception that a 76 mm outside diameter external quartz tube was used, the graphite reaction tube was 6 mm outer diameter, the reactant gas composition was 5 mole % methane, and the annular argon "purge" flow was 1.2 SLM. The adjusted molar concentration of CH_4 accounting for a combined reactant "purge" gas stream near the exit of the graphite reaction tube was 1 mole%. The solar flux was varied at seven different intensities between 1000 and 2540 kW/m^2, with corresponding temperatures in the range of 1480 to 1955 K. The measured hydrogen content in the product gas for each of these conditions showed an increase in methane dissociation over a range of 6% to 43% for a solar flux of 1480 kW/m^2 to 1955 kW/m^2. This set of experiments indicated that different sizes of outer quartz protection tubes could be used and that the extent of dissociation increased with an increase in the solar-flux to the reaction tube.

The reactor apparatus was modified so the graphite reaction tube extended over the entire length of the surrounding protective quartz tube. This design modification kept the reaction contents inside the graphite reaction tube and isolated the graphite reactor contents from the annular space between the graphite tube and the quartz protection tube. A non-oxidizing argon gas flowed in the annular space between the graphite reaction tube and the quartz protection tube to prevent oxidation of the graphite tube. The flow of this non-oxidizing gas also prevented any volatile species emanating from the graphite tube upon heating from depositing on the inside surface of the quartz protection tube. This design also prevented any deposition of carbon particles on the inside surface of the quartz protection tube. The concentrated sunlight passed through the protective quartz wall to the graphite tube outside wall where it heated the graphite tube to reaction temperature.

The outside quartz protection tube had an outside diameter of 25 mm and was 305 mm long. The inside graphite reaction tube had an outside diameter of 10 mm and was also 305 mm long. Inert argon gas flowed through the annular gas flow space at a rate of 3 SLM. Reactant gas comprising 10 mole% methane in argon flowed through the graphite reaction tube at a flow rate of 0.3 SLM. No carbon particles were fed during the run, but, instead were formed during the reaction and provided an in-situ method for providing radiation coupling to heat reactant gas during the processing. A solar flux of 2140 kW/m^2 was used to heat the graphite reaction tube to a temperature of 1835 K. The downstream thermal conductivity detector measured the concentration of hydrogen in the combined reaction product gas/annular "purge" gas stream to be 1.04 mole% H_2. The residence time in the hot zone of the reaction tube was 0.06 seconds. A 58% conversion of CH_4 to carbon black and H_2 was obtained. Inspection of the quartz wall after the run indicated no deposition of carbon black or other species. This example indicates that the surface of the protective quartz wall can be kept clean by extending the graphite reaction tube along the entire length of the surrounding protective tube and isolating the reactor contents from the annular space between the concentric tubes.

The apparatus described above (a graphite tube that extended the length of the quartz tube) was used for this set of experiments. This experiment was run on a very clear day with direct normal irradiance at approximately 1000 W/m^2. As used herein, "irradiance" is defined as the quantity of sunlight coming directly from the sun disk, measured within a cone angle of 5 degrees by a Normal Incidence Pyrrheliometer. The estimated flux on the target was about 2400 kW/m^2 or 2400 suns. The graphite reaction tube temperature was 1910 K.

The flow of annular "purge" argon gas was initiated at 2 SLM, then the particle feed and a 5 mole% methane-in-argon mixture (at a flow rate of 0.1 SLM) were started at about 4 minutes. The time delay for the flow to reach the hydrogen detector was about 20 – 30 seconds. The thermal conductivity of methane is higher than that of argon, indicated by a change in the apparent H_2 mole% trace. When the signal became steady, concentrated sunlight was introduced by opening a fast-acting shutter. A nearly immediate increase can be seen in the percent H_2 trace. The shutter was closed at about 11 minutes, corresponding to a decrease in the H_2 signal at about 11 minutes. At 16 minutes of elapsed time, the flow of methane-in-argon was stopped, then restarted, stopped again, and restarted at 0.2 SLM at 18 minutes elapsed time. The changes in H_2 signal clearly indicate that the hydrogen production is following these flow manipulaitons. A sample bag was filled for subsequent analysis during the interval between about 20 and 25 minutes. The shutter was closed at about 27 minutes.

The gas sample was analyzed by GC and found to be comprised of 0.813 mole% H_2, 183 parts per million (ppm) CH_4, 523 ppm C_2H_4, 183 ppm C_2H_2, and the balance (99.4 mole%) argon. For the flow rates of methane and argon in this experiment, complete conversion of methane to hydrogen would have resulted in 0.91 mole% H_2. Thus, the measured conversion of methane was about 88%. Inspection of the quartz tube wall indicated that no deposition of carbon black or volatile species occurred. This example demonstrates that high reaction temperatures and reaction conversions can be achieved using concentrated sunlight while preventing wall deposition on the protective quartz tube.

The apparatus described above was also used in the study of the dry reforming of methane and carbon dioxide (CO_2) to form hydrogen and carbon monoxide (CO). Like reaction (1), this is a highly endothermic reaction that requires high temperatures to achieve high conversions. During this experiment, the annular argon "purge" flow rate was 2 SLM. The reactant gas was comprised of 0.90 mole% CH_4 (0.2 SLM of 10 mole% CH_4 in argon) and 0.45 mole% carbon dioxide (0.01 SLM of dry CO_2). A gas sample was taken downstream prior to solar-thermal heating and analyzed using a GC. The measured composition of 0.45 mole% CO_2 and 0.84 mole% CH_4 with the balance argon indicated a feed molar composition of CH_4 to CO_2 in the ratio 1.87 / 1. The reactor was heated to a temperature of 1645 K using a solar-flux of 1500 kW/m^2. Carbon black was collected downstream after the run indicating that reaction (1) took place. The downstream product gas (analyzed by GC) was comprised of 0.23 mole% CO_2, 0.20 mole% CH_4, 0.35 mole% CO, and 1.55 mole% H_2, corresponding to a CO_2 conversion to CO of approximately 49%. The experiments were repeated, but with a solar-flux of 2000 kW/m^2 heating the reaction tube to a temperature of 1795 K. A GC analysis of the collected product gas indicated a composition of 0.11 mole% CO_2, 0.07 mole% CH_4, 0.62 mole% CO, and 1.60 mole% H_2, corresponding to a CO_2 conversion to CO of approximately 76%. The fact that large concentrations of H_2 were measured indicates that a significant amount of the excess CH_4 fed according to the dry reforming reaction dissociated according to reaction (1). Carbon black was found in the collection dust filter to further substantiate this observation. This set of examples illustrates that concentrated sunlight can be used to carry out dry CO_2 reforming of CH_4 reactions in short-residence-time (fractions of a second) solar-thermally heated transport graphite reaction tubes.

Improved Experimental Reactor Design

The reactor system is currently being modification and re-designed to eliminate some of the experimental limitations inherent in the proof-of-concept design. The new reactor system will allow us to perform experiments at high concentration of methane. This should allow us to get better kinetic expression results. We will also be constructing a new feeder mechanism in order to provide smoother consistent feeding of particles. The current particle feed system is extremely limited in capacity of feed. The new particle feeder will be capable of continuous operation. There is also a secondary concentrator, which will increase the solar radiation incident upon the graphite tube. The current design only allows at most a 10% solar efficiency. The addition of the secondary concentrator will increase the solar efficiency to 74%. This should increase the temperature that the reactor is capable of achieving.

A process schematic is shown in Figure 16. The particle feeder is a conical screw feeder. The feed particles drop into a jetted stream of process gases. The jets should entrain the small graphite powders into a fine aerosol of powders. This aerosol flows into the top of the graphite tube. The graphite will heat with the solar radiation and this will in turn heat the graphite powders. The fine aerosol of powders will in turn heat the gases. Methane will crack into H_2 and C. The C will be removed in a filter housing. The product gases will be analyzed for composition by an in-line GC/MS. A dry test meter will measure the volume of product gases. The will allow quantification of reaction conversion. Outside the graphite tube, a quartz tube contains a cooling

gas. This gas is inert for safety reasons. The inert annular gas will not mix with the process gases.

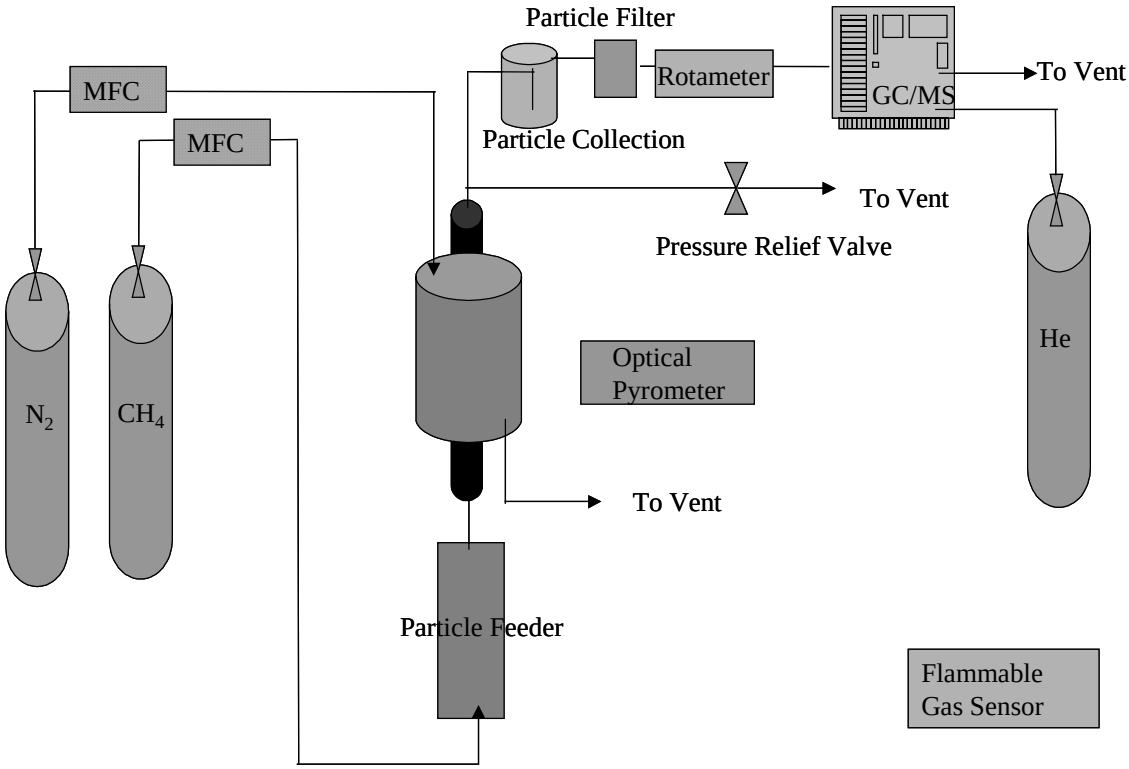

Figure 16. Process Flow Schematic of Improved Experimental Reactor

The reactor itself (Figure 17) consists of a glassy carbon graphite tube inside a quartz tube. The two tubes are sealed at the ends with custom fittings designed to have small clearance in order to reduce the excess length of the reactor. Two sizes of graphite tubes will be investigated, 2.4 cm and 1.2 cm outer diameter with a wall thickness of 3 mm. The total length of the reactor is 15 inches. There are four silicone O-ring seals on each end of the reactor that prevent leaking of gases into the atmosphere as well as mixing of the two gas streams. The gas inlets and outlets will be fitted with VCR-type fittings. These connections will have to be opened frequently and the VCR fittings provide positive seal when a new gasket is used each time the fitting is closed.

Rudimentary heat transfer modeling of the proposed reactor design was performed in order to determine if the selected materials were appropriate for construction. It was assumed that the graphite tube was 2000°C at the center portion while the gases entered that portion at room temperature. The outlet temperature of the graphite and the quartz were predicted based on co-current plug flow of gases, uniform radial temperature through the quartz and graphite, and no radiative heat losses. This model predicted that the process gases would quickly reach the temperatures we desire for reaction (~2000°C). The ends of the graphite tube reach about 300°C, which is below the maximum operating temperature of the silicone O-rings of 370°C. The model

predicts that the quartz will remain at or below 1000°C indicating that there shouldn't be problems with it softening and deforming.

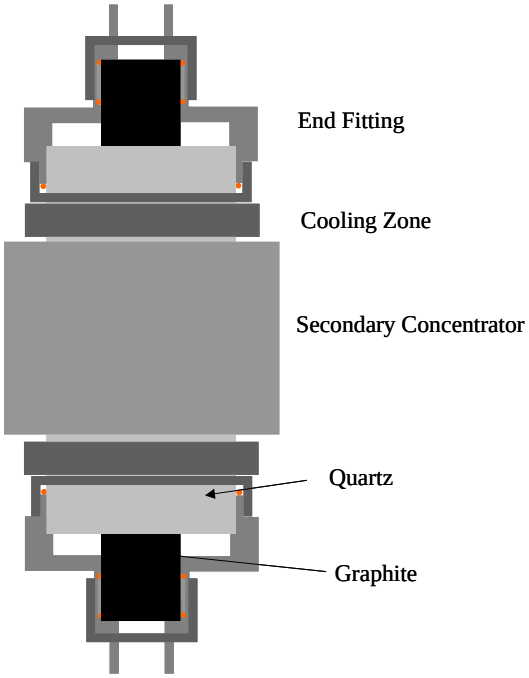

Figure 17. Schematic of Improved Experimental Reactor

Actual operating conditions should be more effective at protecting the seals and quartz. The process will be run in counter-current flow conditions. This will pre-heat the reacting gases allowing them to reach temperature faster, as well as cooling the gases and tubes more effectively at the ends. Radiative heat losses will also prevent the thermal build-up in the reactor system. In addition, we have designed two small water cooling sections on the outside of the quartz on either side of the heated secondary concentrator zone. These will contact cooling water with the quartz walls to draw a lot of heat out of the system.

The secondary concentrator was designed to optimize the radiation at the HFSF. Optics and Energy Consultants, Inc. (Muenchen, Germany) started with the ray tracing measured off of the primary concentrator. Then they structured the planes of the V-cone concentrator to optimize the reflection and focusing of the sunlight onto the front of the graphite tube. The predicted energy impinging upon the graphite tube is shown in Figure 18. The trough portion of the concentrator will focus the leaked light on the back of the tube. The design optimizes reflection of the radiation from the primary concentrator to evenly irradiate the center of the graphite cylinder. The predicted losses of energy are shown in Figure 19. This design increases the solar efficiency from 10% without a secondary concentrator to 74% with the secondary concentrator and the larger graphite tube. The smaller graphite tube shows more uniform illumination on the backside as seen in Figure 18. However, the increased losses reduce the energy efficiency to 47 %.

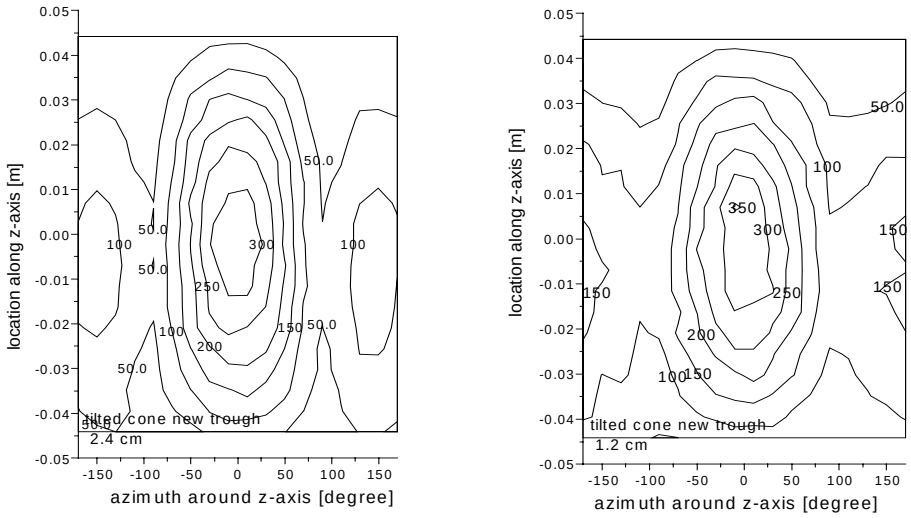

Figure 18. Distribution and Intensity of Solar Radiation on Graphite Tubes

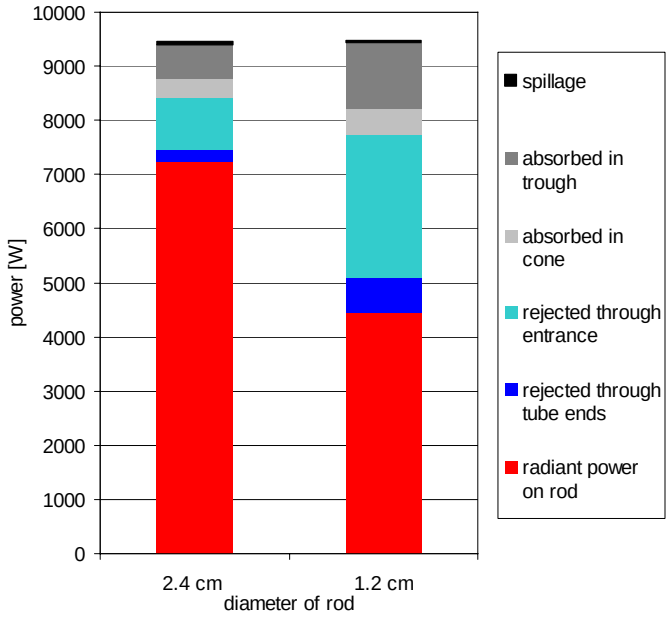

Figure 19. Predicted Energy Distribution Through Improved Experimental Reactor

A schematic of the secondary concentrator is shown in Figure 20. The secondary concentrator will be constructed out of aluminum plates. Final polishing of the surfaces will create an optically smooth surface. Denton Vacuum will coat the plates in a vacuum deposition process. Each individual plate will have cooling channels cut into the back side, with a cooling water inlet and outlet. This will prevent heat from building up in the reflector and damaging the coating on the inside.

The particle collection container is a micro filter that collects all of the powders while allowing the gases to pass through. This is a large-surface-area filter, which should not clog except under very high particle loading. The filters can be easily changed between runs so that particle morphology can be studied as a function of reaction conditions.

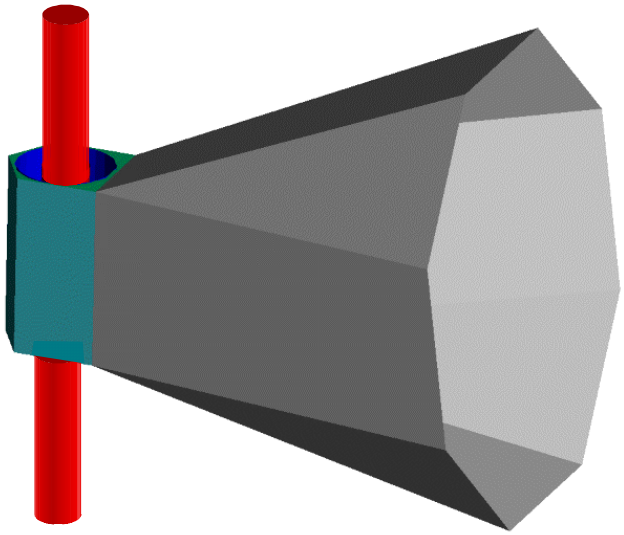

Figure 20. Schematic of Secondary Solar Concentrator

An Inficon (East Syracuse, NY) Hapsite GC/MS system will be used to measure the concentration of different gases in the reagent and product streams. The GC will be equipped with a 27 m x 0.32 mm Carboxen 1010 capillary column (Supelco, Bellafonte, PA). This will allow for separation of the light gas compounds. Helium will be used as the carrier gas. This prevents interference of N_2 (normally used with the Hapsite for portability) with CO during the MS analysis. The quadrupole mass spectrometer should be capable of measuring ppm levels of light gases in the samples. Concentrations much higher than that are anticipated in the product stream. The Hapsite was chosen for these studies due to its stability. It was designed to be used as a portable GC/MS unit. While this application does not require a portable field unit, it does require a low-drift instrument.

This new design addresses all of the experimental deficiencies in the previous design. Since the flammable gas stream was only contained in glass, safety concerns prevented study of high concentration of reactant. The new design separates the flammable gas from the glass with a glassy carbon tube, which is completely sealed from the inert gas passing between the quartz and graphite. The old reactor did not allow for in-line quantification of the product gases. The GC/MS will allow semi-continuous and quantitative monitoring of the product stream composition. Volumetric flow rate measurements of the product stream will allow a mass balance to be closed.

Process Design and Cost Analysis

A preliminary plant design was developed for a solar-coupled process for the thermal decomposition of methane to hydrogen and carbon black. The process economics were evaluated using discount cash flow analysis. Cash flow analysis determines the required selling prices of the hydrogen and carbon black products. The sales price of these products must generate sufficient revenue to pay for annual operating expenses and the initial capital investment, and provide an acceptable internal rate of return over the lifetime of the process.

Since some of the specific design factors and process costs were not known exactly, these factors and costs were treated as parameters in the analysis. This approach provides insight into how the process economics depend on the values of these factors and costs, and determines which factors and costs are most important in determining the overall process economics.

A preliminary evaluation of the current carbon black commercial market was also performed to determine current market sizes for the various grades of carbon black products and their corresponding selling prices. Results from the process design, economic analysis, and market evaluation were used to draw conclusions and make recommendations for future research and process development.

Process Plant Design

The solar-coupled plant is envisioned to have many of the same unit operations as those of a current commercial carbon black plant [Wang, 1993]. A schematic of the plant is shown in Fig. 21. The reactor is mounted on top of the tower that receives concentrated solar from a field of tracking mirrors or heliostats. The concentrated solar energy provides the energy needs for the process and eliminates the need for partial combustion of the feed. The feed for this process is natural gas, which is preheated in the heat exchanger by the product stream. Natural gas, recycled hydrogen and carbon particles enter the top of the reactor and flow downward where they are heated directly with solar flux. Decomposition of the natural gas results in a product stream consisting of carbon black and hydrogen.

A water quench is not used in this design to maintain a pure stream of carbon black and hydrogen. The product stream flows through the tube side of the heat exchanger and is cooled to about 200^{o}C (473 K) before entering the bag houses. The carbon black is separated in the bag houses and transferred to the storage tanks in the same manner as that of the commercial carbon black process. Hydrogen gas exits the top of the bag houses at near-ambient temperature and pressure. A portion of the hydrogen gas is recycled back to the reactor and fed separately to flow past the reactor window and prevent deposition of carbon black. This process design and analysis does not include unit operations for the compression and storage of the hydrogen gas product.

Operation of a solar-coupled plant will be continuous but will only operate when sufficient solar irradiance is available. This fraction of time is referred to as the solar capacity factor and varies with geographic location. Capacity factors for locations that are favorable for solar processes, such as the desert southwest portion of the United States, have been measured to be as high as 0.41. For this work, the capacity factor was varied from 0.28 to 0.41. Limited operation of the

solar-coupled plant results in higher capital costs as compared to a continuous operation plant with the same annual production capacity.

a.

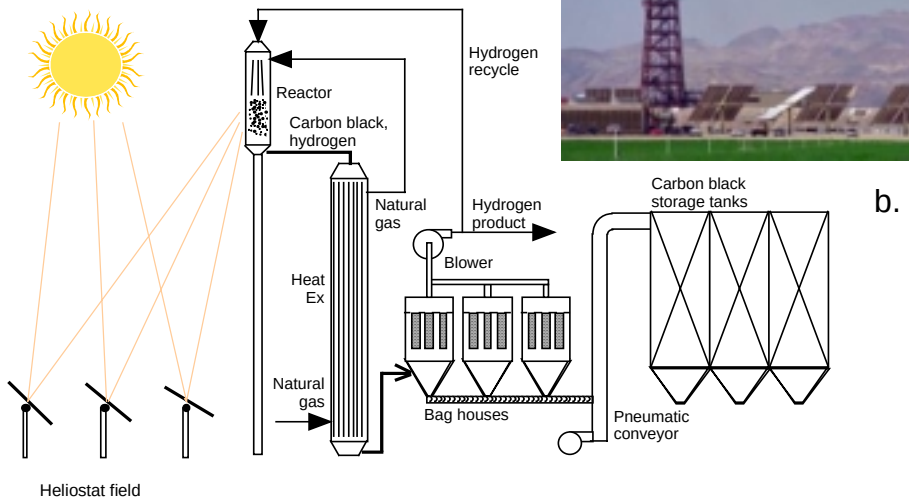

b.

Figure 21. Solar-Thermal Processing: a. schematic of aerosol CH_4 dissociation process, b. photograph of 10 MW Barstow, CA facility

Cash Flow Analysis

Cash flow analysis was performed to determine process economics for the solar-coupled process. The analysis consisted of determining the fixed capital and annual operating costs for the process as a function of several cost parameters. These parameters included heliostat cost, reactor thermal efficiency, and the cost of natural gas. The methods for determining capital and operating costs are described previously [Weimer, et.al., 2000]. Capital and operating costs for each case were used in the cash flow analysis to determine the required selling price for hydrogen.

All material & energy balances and cost calculations were performed using a Microsoft Excel® spreadsheet. The spreadsheet that was developed previously included calculations for discount cash flow over the lifetime of the process. These calculations were used to determine the required selling price for hydrogen for a given set of parameter values. The spreadsheet was structured such that values of the hydrogen price had to be assigned in the spreadsheet until the correct value produced the proper cumulative discount cash flow. This “trial & error” method was replaced by restructuring the spreadsheet so that the required price for the hydrogen product is calculated explicitly. User-defined functions were written to perform the search for the correct hydrogen price value for a given set of parameter values.

The current cash flow analysis has the assumptions listed in Table 2.

Table 2. Economic Assumptions for the Discount Cash Flow Analysis

Economic Factor	Value
Internal Rate of Return	15%
Depreciation	see Table 3
Recovery Period	11 years
Plant Life	21 years
Construction Period	1 year
Working Capital	18% of Fixed
State Tax	5% of net income
Federal Tax	see Table 3
Salvage Value	10% of Fixed
Debt/Equity Ratio	0/100
Cost of Labor	$34/hr (loaded)
Reference Year for Costs	2000

Depreciation occurred over the first 11 years of plant operation according to Table 3 [Seider et al., 1999].

Table 3. Depreciation Schedule

Year	Percent of Capital Depreciated
1	10.00
2	18.00
3	14.40
4	11.52
5	9.22
6	7.37
7	6.55
8	6.55
9	6.56
10	6.55
11	3.28

Federal tax for the net income was calculated according to the schedule in Table 4. The total tax was determined by applying the appropriate tax rate to each range of income. For example, to determine the tax on a net income on $120,000, the first $50,000 is taxed at 15%, the next $25,000 is taxed at 25%, the next $25,000 is taxed at 34%, and the last $20,000 is taxed at 39%.

Table 4. Federal Tax Schedule

Net Income (K$)	Tax Rate (%)
< 50	15
50 to 75	25
75 to 100	34
100 to 335	39
335 to 10,000	34
10,000 to 15,000	35
15,000 to 18,300	38
> 18,300	35

Cash flow analysis determined the required selling prices of hydrogen and carbon black to achieve a net present value of zero at the end of the lifetime of the process. This approach is consistent with the method used by the Hydrogen Program to assess the economics of hydrogen production processes [Mann, 1995]. For all cases, the hydrogen that was produced was assumed to have an energy content of 39.4 kWhr/kg (0.0611 MBtu/lb), which corresponds to its higher heating value (HHV). The final hydrogen product was at ambient temperature and pressure.

Capital Cost Estimation

The capital equipment items for the process included the land, heliostats and tower, reactor, heat exchanger, bag houses, pneumatic conveyor, blower, and storage tanks. For each item, a purchase cost was determined. Methods for calculating purchase costs for each item have been described previously [Weimer, et.al., 2000]. The purchase cost included shipping and sales taxes. The fixed capital cost for each item was determined by multiplying the purchase cost by an inflation factor, a set of direct and indirect cost factors, and a contingency and fee. The only change to the methods for calculating equipment purchase costs was for the solar reactor.

The reactor was assumed to be a vertical cylindrical design consisting of a graphite cylinder enclosed within an outer quartz cylinder. The quartz cylinder is supported inside a steel housing. A portion of the length would not have the steel housing and would function as the window. Reactant flow is through the graphite cylinder. The quartz outer cylinder is included to thermally shield the graphite reactor and to prevent oxidation of the graphite during operation. The graphite cylinder volume is determined from the volumetric flow rate at reaction temperature and pressure and the required residence time. Since the molar and volumetric flow rates increase as the decomposition of methane proceeds, these flow rates were based on product flow rates. The quartz volume was determined assuming a gap between the graphite and quartz cylinders was 0.13 meters.

The purchase cost was based on cost estimates obtained from a local vender for quartz tubing having diameters of 1, 2, 2.5, 3, and 3.5 ft. For all sizes, the cost of the quartz tubing, on a volume basis, varied from \$900/ft^3 to \$1,200/ft^3. The purchase cost of the reactor was chosen to be \$1,100/ft^3 or \$38,870/m^3. The purchase cost of the reactor was assumed to be linear with reactor volume. The purchase cost of the graphite cylinder was assumed to be \$300/ft^3. An additional factor was included for the cost of the steel housing.

The estimated cost for heliostats varies widely depending on the size of the plant and state of maturity of the solar industry. For this reason, heliostat cost was made a parameter in this analysis. The overall heliostat field efficiency accounts for reflectivity losses (about 5%), projected area losses due to the angle between the incident sunlight and the target reactor and soiling due to dust and dirt. Values for this efficiency vary depending on the location of the heliostat and tower relative to the position of the sun in the sky. An average value for all of the heliostats was assumed to be 0.69. Resource is the average solar resource that is available when the plant is operating. For this analysis, the solar resource was assumed to be 0.75 kW/m^2.

The operating and maintenance (O&M) costs were determined for the process. The process was assumed to require a staff of 3 operators during operation. In addition, several labor hours were included for each process item for maintenance and repair. For each item, the number of labor hours per day or per some measure of equipment size or production capacity was estimated. The fully-burdened rate for all labor was $34/hour. Supervision labor was estimated at 15% of the total O&M labor. Since the price of natural gas has varied dramatically in the past year, the cost of natural gas was evaluated as a parameter.

Base Case

A base case for the process was developed in which the most likely values for the parameters were used. A production capacity of 5,000,000 kg/yr was chosen because this capacity requires about 16 MW of power to be delivered to the reactor. This corresponds to about half the power that is delivered to the receiver at the solar thermal electric power plant in Barstow, California. Cash flow analysis determined the required selling prices of hydrogen and carbon black to achieve a net present value of zero at the end of the process lifetime. The parameter values for the base case are given in Table 5.

Table 5. Parameter Values for the Base Case

Parameter	Value
Annual hydrogen production	5,000,000 kg/yr
Heliostat cost	$200/$m^2$
Fraction of hydrogen recycled	0.2
Reactor temperature	2,000^oC (2273 K)
Reactor residence time	0.1 second
Reactor thermal efficiency	0.5
Solar capacity factor	0.28
Cost of natural gas	$3/1000 scf

A summary of the equipment size and equipment fixed capital cost according to equation for each piece of equipment is included in Table 6 for the base case of 5,000,000 kg H_2/yr. The total equipment fixed capital investment is $26,300,000 and total capital required is $31,000,000.

Table 6. Summary of Fixed Capital Equipment Cost (Base Case)

Equipment	Size*	Purchase Cost*
Land:	370,000 m^2	$185,000
Heliostat:	61,700 m^2	$12,300,000 (installed)
Tower:	79 m	$590,000 (installed)
Reactor:	16 MW_{th}	$460,000
Heat Exchanger:	5,200 m^2	$360,000
Baghouse Filter:	590 m^2	$69,000
Other Equipment		
Pneumatic Conveyer:	1000 kg/hr	Other Equipment Total:
Storage Tanks:	115 m^3	$686,000
Blower:	2.4 m^3/s (5,000 scfm)	
Total Equipment:		$14,700,000
Installation:	Direct + Indirect	$11,600,000**
Fixed Capital Investment		$26,300,000
Working Capital	18%	$4,700,000
Total Capital		$31,000,000
	* Rounded for clarity	**other than heliostat and tower

Cash flow analysis determined the required selling prices of hydrogen and carbon black to achieve a net present value of zero at the end of the lifetime of the plant.

Various price combinations for hydrogen and carbon black were determined. The extreme cases are hydrogen sales only where the price of carbon black is $0/kg and carbon black sales only where the hydrogen price is $0/kWhr. For the intermediate cases, the price for carbon black was set and the required price for hydrogen was then determined. A summary of these results is presented in Table 7.

Table 7. Required Sales Prices for Hydrogen and Carbon Black for Base Case.

Carbon Black Price ($/lb)	Hydrogen Price ($/MBtu)
0.00	23.26
0.10	18.35
0.20	13.44
0.30	8.53
0.40	3.62
0.48	0

Results show that if only hydrogen is sold, the price must be $23/Mbtu. If only carbon black is sold, the price must be about $0.48/lb.

Parametric Analysis

The selling prices for hydrogen and carbon black were determined for variations of the base case in which the parameter values were varied one at a time. Each of the following parameter variations assumes a different fixed price for the carbon black. As a result the relative impacts of the parameter are the important result rather than the absolute values.

Increasing the reactor temperature also increases total gas volumetric flow through the reactor. When the reactor temperature is changed from 1500^{o}C to 2200^{o}C, the hydrogen price ranged from $2.3-4.2/MBtu at a carbon black price of $0.40/lb. Decreasing the reactor residence time appears to be practical based on the reaction kinetics. When residence time ranges from 0.05 to 1 second, the hydrogen sales price ranges from $17.7-26.5/MBtu at a carbon black sales price of $0.10/lb.

When the size of the plant was increased from 1,000,000 kg/yr to 10,000,000 kg/yr, the required sales price of hydrogen went from 17.9/MBtu to 15.4/MBtu at a fixed cost of carbon black of $0.15/lb.

The cost of heliostats is uncertain because the technology and the market are still developing. This cost was varied from $100/m^2 to $500/m^2 with a resulting price of hydrogen of $10-23/MBtu at fixed cost of carbon black of $0.20/lb.

Decreasing the reactor thermal efficiency increases the thermal energy requirement for the reaction, and therefore, the size of the heliostat field. Decreasing this efficiency from 0.7 to 0.2 increased the sales price of hydrogen from $5.5-$24.7/MBtu at a sales price of carbon black of $0.30/lb.

The cost of natural gas is increasing in the current market. At a fixed cost of carbon black of $0.40/lb increasing natural gas cost from $3/1000scf to $10/1000scf results in an increase in the price of hydrogen from $3.6/Mbtu (base case) to $14.9/MBtu.

The profitability analysis is summarized in Figure 22. The effect of residence time, plant size, heliostat cost, reactor efficiency and natural gas cost on required hydrogen selling price is shown at arbitrary, fixed values of carbon black selling price.

Clearly, reactor efficiency is an important parameter in achieving overall system performance and acceptable hydrogen selling prices. This is also an engineering parameter that should be, and is, the focus of the technology development within this project. Tied to reactor efficiency is the residence time. Although driven primarily by the attractive kinetics of this reaction, the reactor must be designed to allow effective heat transfer to the reactants for the kinetics to take place.

In the range of reasonable solar thermal plant sizes, it appears that there is relatively little economy-of-scale. Starting with a smaller plant size in the development phase of the project will have small impact on the price of hydrogen. As solar thermal technology for other applications (power plants, etc.) grows, the cost of heliostats will be reduced. This cost is mostly driven by

outside influences and will be tracked as the technology develops. This is also true for the cost of natural gas.

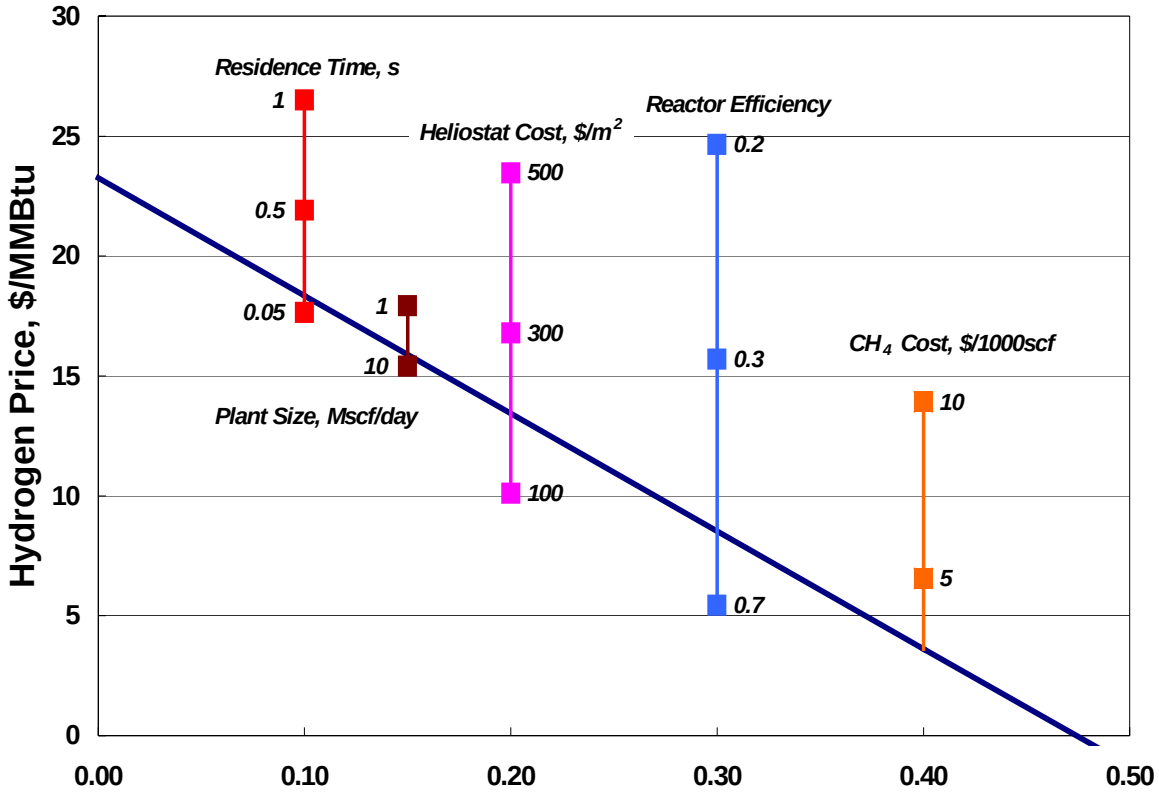

Figure 22: Profitability Analysis

By far the largest influence on the price of hydrogen is the sale of the second reaction product, carbon black (see Figure 23). If high quality carbon black from this process can be sold for significantly more than the current market price for bulk carbon black for the tire market, then this dominates the overall economics and hydrogen almost becomes irrelevant. However, if hydrogen is sold for the current market value (based on other production technologies) then the profitability of this process can be significantly increased (i.e., higher IRR).

Energy Efficiency

An overall energy efficiency was determined for the process. The efficiency is defined as the quantity of energy captured by the methane decomposition reaction due to the heat of reaction divided by the quantity of energy incident on the heliostat field. The efficiency accounts for optical losses of the heliostat field and the thermal efficiency of the reactor. It also accounts for the fact that a portion of the energy delivered to the reactor is use to heat the reactants to the

reaction temperature. Overall efficiencies were determined for the base case with reactor thermal efficiencies of 0.3, 0.5, & 0.7. One can also determine the ratio of the quantity of energy available in the hydrogen product divided by the quantity of energy required to make the hydrogen from methane. Results are presented in Table 8.

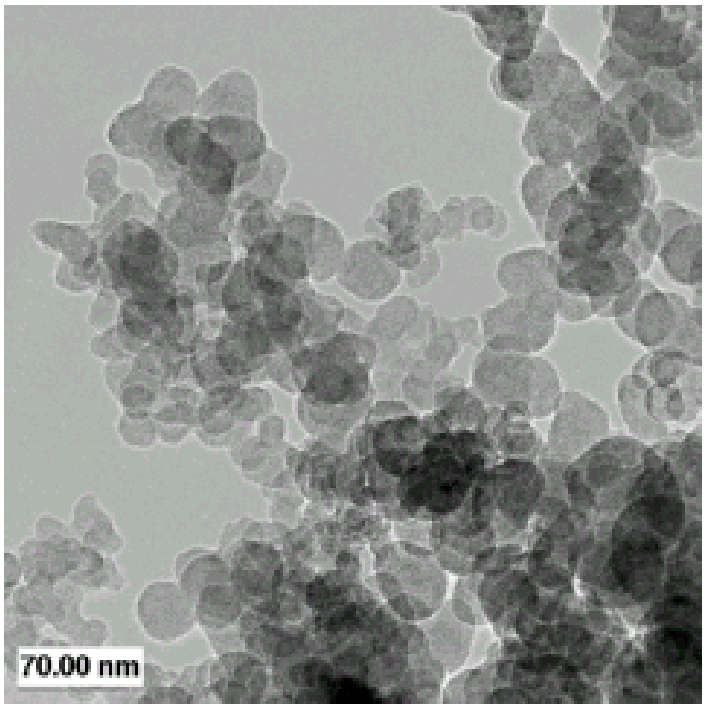

Figure 23. 20 to 40 nm Sized Amorphous Carbon Black Formed By Methane Solar-thermal Decomposition

Table 8. Energy Efficiencies and Available Product Energies

Reactor Thermal Efficiency	Process Energy Efficiency	Ratio of Energy Available to Energy Used
0.3	0.170	1.04
0.5	0.283	1.74
0.7	0.396	2.43

Market Analysis for Carbon Black

A preliminary evaluation of the current carbon black commercial market was also performed to determine current market sizes for the various grades of carbon black products and their

corresponding selling prices. Applications for carbon black include the reinforcement of rubber, use as black pigment, and as a conductive additive to rubber and plastic products [Kirk-Othmer, 1991]. World production of carbon black in 1989 was greater than 6 million metric tons. United States production was about 1.6 million metric tons. About 70% of the carbon black that is produced is used in the reinforcement of rubber for tires, 20% is used in other rubber products, and the remaining 10% in non-rubber products. Carbon black used for rubber reinforcement sells for about $0.30/lb to $0.35/lb [Chemical Marketing Reporter, 2000].

The non-rubber applications include additives to plastics, printing inks, paint, and paper. A special electrically conductive grade of carbon black sells for prices that are considerably higher than those that are used in rubber reinforcement. Electrically conductive grades are used to produce conductive and antistatic polymer composites. Applications include antistatic carpeting, floor tile, heating elements, videotapes and disks, and electrical shielding. Markets for these applications are increasing faster, on a percentage basis, than those for conventional uses. The current price for a higher grade of carbon black (Thermax) is $0.78/lb [Canadian Carbon Company, 2000]. An even higher grade of carbon black produced from acetylene sells for $1.40/lb [Chevron Chemical Company, 2000].

In 1989, the total market for specialty-grade carbon blacks was 126,000 metric tons or 126,000,000 kg. A solar-coupled hydrogen production plant that produces 5,000,000 kg/yr of hydrogen will produce 3,000,000 kg/yr of carbon black. This represents about 10% of the current United States market for higher-grade carbon blacks. The addition of this production capacity to the current market would not have a significant impact on the price of higher-grade carbon blacks and as this market is increasing faster than other carbon black markets, demand for the additional production capacity should be easy to identify.

Life Cycle Assessment

To evaluate the environmental impact of the solar thermal methane dissociation plant, we performed a preliminary life cycle assessment (LCA), on a limited number of process blocks within the system. Life cycle assessment (LCA) is an analysis that provides an evaluation of the environmental impacts associated with a product, process, or activity. This assessment identifies material and energy consumption, as well as pollutants released to the environment because of the process [www.life-cycle.org/]. Although hydrogen is a clean fuel and the process of solar thermal dissociation of methane itself is also a clean process, there are various polluting processes that are associated with a real-life implementation of the process. An LCA provides a cradle-to-grave perspective on the system that incorporates the environmental impacts of the associated processes. While this preliminary LCA provided us a framework for evaluating the environmental benefits of this process, a more detailed assessment is required for determining actual impacts. Results to-date indicates that significant reductions in greenhouse gas emissions and system energy consumption are possible. Future studies will expand the boundaries to include all operations required for the solar-thermal driven aerosol reactor to operate. Additionally, a more complete LCA study will allow us to compare this system with steam methane reforming.

Summary and Conclusions

The objectives of this work were to carry out "proof-of-concept" experiments at the NREL HFSF, develop a fundamental understanding of methane thermal dissociation kinetics, develop an improved process design for a solar-thermal process, evaluate the process economics using discount cash flow analysis, and carry out a life cycle assessment of the process compared to conventional steam reforming to produce hydrogen. The initial results are encouraging and have demonstrated that the process works in principle.

High methane dissociation conversions have been achieved using a solar-thermal reactor not designed for the specific process and using only modest solar concentration levels. In addition, solar-thermal dry reforming has been demonstrated for the conversion of contaminated with CO_2 natural gas sources to produce useful syngas. The Phase 2 experimental system has been designed and is being constructed. It eliminates the deficiencies that are inherent in the current reactor system (low solar efficiency and low feed concentrations) and allows for more complete quantification of products. A secondary solar concentrator having solar-thermal efficiencies approaching 75% with an in-line GC/MS and volumetric flow rate measurements will allow material balance closure and better definition of the overall process that are needed for scale-up. Reactor temperatures of 2000^{o}C can be obtained and pure methane and natural gas can be decomposed.

The conceptualized plant design includes the same major equipment components as current commercial carbon black production plants. These components include a high-temperature reactor, heat exchanger, bag house filters, pneumatic conveyor, blower, and storage tanks. In addition, the process includes a solar heliostat field and tower to provide the thermal energy needs of the process. The process design and economic analysis contain enough refinement to determine how the price of hydrogen and carbon black vary with the values of several key process parameters and costs. Parametric analysis provides insight into how the process economics depends on the values of these factors and costs and determines which factors and costs are most important in determining the overall process economics.

Results of the discount cash flow analysis show that the required single-product selling price for hydrogen for the base case 5,000,000 kg/yr hydrogen plant is $23/MBtu and for carbon black is $0.48/lb. These prices assume that only one product is sold. If both products are sold, then the selling price for each decreases. For example, selling prices of $13.4/MBtu for hydrogen and $0.20/lb for carbon black meet the discounted cash flow requirements (15% IRR).

The selling prices were determined as a function of several parameters that are not well established at this point in the development of this process. Some are technical in nature and can be influenced by the results of this project (residence time and reactor efficiency) and others are influenced more by outside markets (heliostat cost and natural gas cost). Clearly, the reactor efficiency is the most significant parameter and designing an effective and efficient reactor should be a primary activity within this project.

A preliminary evaluation of the current carbon black commercial market was also performed to determine current market sizes for the various grades of carbon black products and their corresponding selling prices. About 90% of the carbon black that is produced worldwide is used for rubber reinforcement. About 10% is considered specialty-grade carbon black and is used as additives in plastics, printing inks, paint, and paper. The current price for a higher grade of carbon black is about $0.78/lb ($1.72/kg). A solar-coupled hydrogen production plant that produces 1,000,000 kg/yr of hydrogen, will produce about 2.4% of the current United States market for higher-grade carbon black. Since this market is increasing faster than other carbon black markets, demand for the additional production capacity should be easy to identify.

Alternatively, a fine carbon black boiler could be interfaced to the process to burn produced carbon black to generate electricity. Although it is more desirable to sell the carbon black into the carbon black market, it may be feasible to take advantage of the fact that the solar-thermal process increases the energy content of the fuel (resulting C and H_2 heating values relative to starting CH_4 heating value) by about 10%. The fine, high-purity carbon black could be produced at fast rates and stock-piled when the solar-thermal process is operating. A carbon black boiler process with minimal air pollution equipment could then be used to burn carbon black on a continuous basis while hydrogen is supplied intermittently to an on-site fuel cell process for generating electricity and/or sent by pipeline or tube trailors to transportation centers for use.

The encouraging experimental results, attractive economic analysis, and benign processing indicate that this process warrants further investigation. The sensitivity of the hydrogen selling price to reactor efficiency and heliostat cost points out the need to focus on reactor/secondary concentrator design and performance in the next stages of the project.

Acknowledgements

The authors want to thank the DOE Hydrogen Program and The University of Colorado for financially supporting this work under Grants DE-FC36-99GO10454 and DE-PS36-99GO10383.

References

Bale, C.W., A.D. Pelton, W.T. Thompson, J. Melançon, S. Degterov, and G. Eriksson. 1999. Facility for the Analysis of Chemical Thermodynamics.

Bromberg, L., D. Cohn, and A. Rabinovich. 1998. “Plasma Reforming of Methane,” *Energy & Fuels*, 12, 11-18.

Canadian Carbon Company. 2000. Personal Communication. Cancarb Limited, 1702 Brier Park Crescent NW, Medicine Hat, Alberta, Canada T1A 7G1 (www.CanCarb.com).

Chapra, S.C. and R.P. Canale. 1988. *Numerical Methods for Engineers.* New York; McGraw Hill.

Chemical Engineering. 2000. McGraw-Hill Publishing Co. (New York).

Chemical Marketing Reporter. 2000.

Chevron Chemical Company. 2000, Personal Communication, Houston, TX

Donnet, J.B. 1976. Carbon Black, 16-18, Marcel Dekker, New York.

Gaudernack, B. and S. Lynum. 1996. "Hydrogen Production from Natural Gas Without Release of CO_2 to the Atmosphere," *Proceedings of the 11th World Hydrogen Energy Conference,* 511-523, Coco Beach, Florida (June, 1996).

Himmelblau, D.M. 1970. *Process Analysis by Statistical Methods.* New York; John Wiley & Sons.

Jenkins, D., R. Winston, J. O'Gallagher, C. Bingham, A. Lewandowski, R. Pitts, and K. Scholl. 1996. "Recent Testing of Secondary Concentrators at NREL's High-Flux Solar Furnace," *ASME J. of Solar Energy Engineering,* 29-33.

Kirk-Othmer Encylopedia of Chemical Technologies. 1991. 4th ed., 4, 1037-1072, John Wiley & Sons.

Kreith, F. and W.Z. Black. 1980. *Basic Heat Transfer.* New York; Harper and Row.

Lee, K.W., W.R. Schofield, and D. Scott Lewis. 1984. "Mobile Reactor Destroys Toxic Wastes in Space," *Chemical Engineering,* 46 – 47, April 2, 1984.

Lewandowski, A. 1993. "Deposition of Diamond-Like Carbon Films and Other Materials Processes Using a Solar Furnace," *Mat. Tech.*, 8, 237-249.

Lewandowski, A., C. Bingham, J. O'Gallagher, R. Winston, and D. Sagie. 1991. "Performance Characteristics of the SERI High-Flux Solar Furnace," *Solar Energy Materials*, 24, 550-563.

Mann, M.K. 1995. "Technical and Economic Assessment of Producing Hydrogen by Reforming Syngas from the Battelle Indirectly Heated Biomass Gasifier," *NREL/TP-431-8143*, 10-13.

Matovich, E. 1977. "High Temperature Chemical Reaction Processes Utilizing Fluid-Wall Reactors," *U.S. Patent 4056602* (Nov. 1, 1977).

Mischler, D., R. Pitts, C. Fields, C. Bingham, M. Heben, and A. Lewandowski. 1997. "Solar Production of Fullerenes from a Powdered Graphite Source," *presented at the International Symposium on Solar Chemistry*," Villigen, Switzerland, October 6-7.

Peters, M.S. and K.D. Timmerhaus. 1991. Plant Design & Economics for Chemical Engineers, 4th ed. McGraw-Hill, Inc. (New York).

Pohleny, J.B. and N.H. Scott. 1962. "Method of Hydrogen Production by Catalytic Decomposition of a Gaseous Hydrogen Stream," Chemical Engineering, 69, 90-91.

Pitts, J.R., E. Tracy, Y. Shinton, and C.L. Fields. 1993. "Application of Solar Energy to Surface Modification Processes," *Critical Reviews in Surface Chemistry*, 2 (4), 247.

Roberts, F., R.F. Taylor, and T.R. Jenkins, ed. 1971. *High Temperature Chemical Reaction Engineering.* London; The Institute of Chemical Engineers.

Roine, A. 1997. *Outokumpu HSC Chemistry for Windows Version 3.0.*

Spath, P.L. and M.K. Mann. 2000. "Life-cycle Assessment of Hydrogen Production via Natural Gas Steam Reforming," NREL/TP-570-27637 (Revised November 2000).

Steinberg, M. 1986. "The Direct Use of Natural Gas for Conversion of Carbonaceous Raw Materials to Fuels and Chemical Feedstocks," *Int. J. Hydrogen Energy*, 11, 715-720.

Steinberg, M. 1987. "A Low Cost High Energy Density Carbon Black Fuel Mix for Heat Engines," *Energy Sources*, 9, 161-171.

Steinberg, M. 1994. "Fossil Fuel and Greenhouse Gas Mitigation Technologies," *Int. J. Hydrogen Energy*, 19, 659-665.

Steinberg, M. 1995a. "The Carnol Process for CO_2 Mitigation from Power Plants and the Transportation Sector," *Brookhaven National Laboratory Report BNL 62835*, Upton, NY.

Steinberg, M. 1995b. "The Hy-C Process (Thermal Decomposition of Natural Gas) Potentially the Lowest Cost source of Hydrogen with the Least CO_2 Emission," *Energy Convers. Mgmt.*, 36 (6-9), 791-796.

Steinberg, M. 1998. "Production of Hydrogen and Methanol from Natural Gas with Reduced CO_2 Emission," *Int. J. Hydrogen Energy*, 23, 419-425.

Steinberg, M. 1999. "Fossil Fuel Decarbonization Technology for Mitigating Global Warming," *Int. J. Hydrogen Energy*, 24, 771-777.

Steinberg, M. and H.C. Cheng. 1989. "Modern and Prospective Technologies for Hydrogen Production from Fossil Fuels," *Int. J. Hydrogen Energy*, 14, 797-820.

Touloukian, Y.S., P.E. Liley, and S.C. Saxena. 1970. *Thermal Conductivity*. New York; IFI/Plenum.

Touloukian, Y.S., S.C. Saxena, and P. Hestermans. 1975. *Viscosity*. New York; IFI/Plenum.

Turner, J.H., A.S. Viner, J.D. McKenna, R.E. Jenkins, and W.M. Vatavuk. 1987a. "Sizing and Costing of Fabric Filters, Part 1: Sizing Considerations," *JAPCA*, 37 (6), 749-759.

Turner, J.H., A.S. Viner, J.D. McKenna, R.E. Jenkins, and W.M. Vatavuk. 1987b. "Sizing and Costing of Fabric Filters, Part 1: Costing Considerations," *JAPCA*, 37 (9), 1105-1112.

Wang, J. 1993. Carbon Black (2^{nd} ed.), Marcel Dekker.

Weimer, A.W., ed. 1997. Carbide, Nitride, and Boride Materials Synthesis and Processing. London; Chapman & Hall.

Weimer, A., J. Dahl, J.Tamburini, A. Lewandowski, R. Pitts, C. Bingham, G. Glatzmaier. 2000. “Thermal Dissociation Of Methane Using A Solar Coupled Aerosol Flow Reactor”, Proceedings of the 2000 DOE Hydrogen Program Review, NREL/CP-570-28890

Warren, D. S., Seader, J. D., Lewin, D. R., *Process Design Principles, Synthesis, Analysis, and Evaluation*, John Wiley & Sons, 392-393 (1999).

Yaws, C.L. 1999. *Chemical Properties Handbook.* New York; McGraw-Hill.

Nomenclature

Variable	Description	Value/Equation	
a	Arbitrary kinetic constant	Eqn. 6	
a_c	Surface area of carbon particle	$3.14x10^{-8}$	m^2
A_i	Cross sectional area of reactor	$4.56x10^{-3}$	m^2
C_{pC}	Heat capacity of carbon	FACT (1999)	J/mol K
C_{pCH4}	Heat capacity of methane	FACT (1999)	J/mol K
C_{pg}	Heat capacity of gas phase	Eqn. 13	J/mol K
C_{pH2}	Heat capacity of hydrogen	FACT (1999)	J/mol K
d_i	Inside diameter of reactor tube	0.076	m
E_a	Reaction activation energy	Eqn. 4	kJ/mol
E_a^*	Transformed reaction activation energy	Eqn. 5	kJ/mol
f	Flow rate of H_2 added through porous walls	$2.36x10^{-3}$	m^3/s (@STP)
F_C	Molar flow rate of carbon	Eqn. 11b	mol/s
F_{CH4}	Molar flow rate of methane	Eqn. 11a	mol/s
F^o_{CH4}	Initial molar flow rate of methane	Varies	mol/s
F_g	Total molar flow rate of gas	$F_{H2}+F_{CH4}$	mol/s
F_{H2}	Molar flow rate of hydrogen	Eqn. 11c	mol/s
g	Multiplying factor times f	43.74f	mol/m s
H_C	Molar enthalpy of carbon	FACT (1999)	J/mol
H_{CH4}	Molar enthalpy of methane	FACT (1999)	J/mol
H_{H2}	Molar enthalpy of hydrogen	FACT (1999)	J/mol
h_p	Convective coefficient between gas phase and carbon particles	Eqn. 9	W/m^2 K
h_w	Convective coefficient between gas phase and reactor walls	Eqn. 10	W/m^2 K
k	Reaction rate	Eqn. 5	s^{-1}
k_g	Thermal conductivity of gas	Eqn. 14	W/m K
k_o	Pre-exponential factor	Eqn. 4	s^{-1}
k_o^*	Transformed pre-exponential factor	Eqn. 5	s^{-1}
L	Length of reactor tube	0.914	m
M_{wC}	Molecular weight of carbon	0.012	kg/mol
M_{wg}	Molecular weight of the gas phase	Eqn. 12	kg/mol
n_c	Number of carbon particles per volume	$\frac{F_c M_{wc}}{v_g A_i V_c \rho_c}$	m^{-3}
R	Gas constant	8.314	J/mol K
R_o	Carbon particle radius	$5x10^{-5}$	m
t	Time	Varies	s
T_C	Temperature of carbon particles	Eqn. 8	K

T_f	Film temperature	$\frac{T_g + T_w}{2}$	K
T_g	Temperature of gas phase	Eqn. 7	K
T_o	Transformation temperature	1200	K
T_w	Reactor wall temperature	Varies	K
V_C	Volume of carbon particle	5.24×10^{-13}	m^3
v_g	Velocity of gas phase	Eqn. 16	m/s
X	Conversion	Eqn. 6	
z	Axial distance through reactor	0<z<L	m

Greek Symbols:

Variable	Description	Value/Equation	
ε_C	Radiative emissivity coefficient for carbon	1	
μ_g	Viscosity of gas	Eqn. 15	Pa s
ρ_C	Density of carbon	2270	kg/m^3
σ	Stefan-Boltzman constant	5.67×10^{-8}	$W/m^2 K^4$